Applied Energy 309 (2022) 118414

Contents lists available at ScienceDirect

Applied Energy

journal homepage: www.elsevier.com/locate/apenergy

# Is bigger always better? Designing economically feasible ocean thermal energy conversion systems using spatiotemporal resource data

Jannis Langer [a,*], Carlos Infante Ferreira [b], Jaco Quist [a]

[a] Delft University of Technology, Faculty of Technology, Policy and Management, Department of Engineering Systems and Services, Jaffalaan 5, 2628 BX Delft, the Netherlands
[b] Delft University of Technology, Faculty of Mechanical, Maritime and Materials Engineering, Department of Process & Energy, Leeghwaterstraat 39, 2628 CB Delft, the Netherlands

## HIGHLIGHTS

- We studied ocean thermal energy conversion's economics under off-design conditions.
- Our design model works for any system size, location, and temperature profile.
- In most analysed cases, conservatively designed systems yield the lowest cost.
- The electricity cost of a 136 $MW_{gross}$ plant are as low as 15.12 US¢(2021)/kWh.
- We give technical and regulatory recommendations to reduce investment costs further.

## ARTICLE INFO

*Keywords:*
OTEC
Modelling
Economic Analysis
LCOE
Off-Design Performance

## ABSTRACT

*Ocean Thermal Energy Conversion (OTEC)* produces electricity using the temperature difference between warm surface and cold deep-sea water. OTEC systems in literature only limitedly consider seasonal seawater temperature variations and thus might not be adequately sized for off-design conditions. This potentially leads to techno-economically sub-optimal design choices. This paper sheds light on which design approach yields the most economically feasible OTEC system considering off-design conditions with 19 years of seawater temperature data in 3-h time steps. We find that systems sized for worst-case thermal resources yield the highest and steadiest electricity production. If seawater temperature variations are moderate, these systems also perform best economically in terms of *Levelized Cost of Electricity (LCOE)*. We demonstrate our model for a 136 $MW_{gross}$ plant in Ende, Indonesia, with an LCOE of 15.12 US¢(2021)/kWh against a local electricity tariff of 15.77 US¢(2021)/kWh. The model is validated for different cost assumptions, system sizes, and temperature profiles to be useful globally. We give recommendations to curb costs and to move large-scale OTEC closer to today's state of the art, e.g. by using multiple smaller seawater pipes instead of few large pipes. The model is useful to prove OTEC's global economic feasibility and to promote the technology's commercialisation.

## 1. Introduction

*Ocean Thermal Energy Conversion (OTEC)* is a renewable energy technology with a large global potential that produces stable baseload electricity with the temperature difference between warm surface and cold deep-sea water. Being at an early development stage, not many things are certain about OTEC's economics. What is certain though, at least for specific system costs, is that *'bigger is better'* [1]. With larger system sizes, specific costs are driven down via economies of scale and OTEC could be cost-competitive against other energy technologies for system sizes above 50 MW [2]. In small island developing states, smaller systems in the range of a few MW might also be economically attractive to decrease their dependency on expensive imported fossil fuels [3]. Therefore, upscaling is key to OTEC's development, especially as current pilot plants are still in the range of some hundred kW [4–6].

The power output of an OTEC plant directly depends on the available thermal seawater resources; the warmer the surface seawater, the more electricity the plant produces [7,8]. Moreover, different sites can be characterised by different deep-sea water temperatures [9]. Considering

* Corresponding author.
*E-mail address:* j.k.a.langer@tudelft.nl (J. Langer).

https://doi.org/10.1016/j.apenergy.2021.118414
Received 8 July 2021; Received in revised form 11 December 2021; Accepted 19 December 2021
Available online 15 January 2022

**Nomenclature**

| Abbreviation | Meaning |
|---|---|
| AC | Alternating current |
| CPI | Consumer price index |
| FRP | Fibre-reinforced plastic |
| HC | High cost |
| HDPE | High density poly ethylene |
| HYCOM | Hybrid coordinate ocean model |
| IUPAC | International union of pure and applied chemistry |
| LC | Low cost |
| OTEC | Ocean thermal energy conversion |

| Symbol | Meaning [Unit] |
|---|---|
| $\Delta$ | Difference - |
| $\varepsilon$ | Effectiveness % |
| $\eta$ | Efficiency % |
| $\lambda$ | Thermal conductivity W/Km |
| $\mu$ | Dynamic viscosity Pa s |
| $\rho$ | Density kg/m$^3$ |
| $b$ | Scale factor - |
| $A$ | Area m$^2$ |
| $AEP$ | Annual electricity production kWh/year |
| $capex$ | Specific capital expenses US$(2021)/[unit] |
| $CAPEX$ | Capital expenses US$(2021) |
| $c$ | Specific heat capacity kJ/kgK |
| $cf$ | Capacity factor % |
| $CRF$ | Capital recovery factor % |
| $d$ | Diameter m |
| $D$ | Distance plant to shore km |
| $DR$ | Discount rate % |
| $Ex$ | Exergy kW |
| $f$ | Friction factor - |
| $h$ | Enthalpy kJ/kg |
| $K$ | Pressure drop coefficient - |
| $l$ | Length m |
| $LCOE$ | Levelized cost of electricity US¢(2021)/ kWh |
| $m$ | Mass kg |
| $\dot{m}$ | Mass flow kg/s |
| $N$ | Number of pipes - |
| $n$ | Project lifetime years |
| $NTU$ | Number of transfer units - |
| $OPEX$ | Operational expenses US$(2021)/year |
| $p$ | Pressure Pa |
| $Pr$ | Prandtl number - |
| $\dot{Q}$ | Heat kW |
| $Re$ | Reynolds number - |
| $s$ | Entropy kJ/kgK |
| $t$ | Thickness m |
| $T$ | Temperature K, °C |
| $U$ | Overall heat transfer coefficient kW/m$^2$K |
| $v$ | Velocity m/s |
| $\dot{W}$ | Power kW |
| x | Vapour quality % |
| $z$ | Roughness mm |

| Index | Meaning |
|---|---|
| $0$ | Reference |
| $cond$ | Condenser |
| $CW$ | Cold water |
| $D$ | Darcy |
| $depl$ | Deployment |
| $des$ | Design & Management |
| $el$ | Electrical |
| $evap$ | Evaporator |
| $ext$ | Extra |
| $gen$ | Generator |
| $HX$ | Heat exchanger |
| $i$ | Year |
| $is$ | Isentropic |
| $L$ | Loss |
| $liq$ | Liquid |
| $log$ | Logarithmic |
| $max$ | Maximum |
| $mech$ | Mechanical |
| $NH_3$ | Ammonia |
| $nom$ | Nominal |
| $p$ | Pressure |
| $pp$ | Pinch Point |
| $sat$ | Saturation |
| $struct$ | Structure & Mooring |
| $t$ | Technical |
| $tot$ | Total |
| $trans$ | Transmission |
| $turb$ | Turbine |
| $W$ | Wall |
| $WW$ | Warm water |

seasonal seawater temperature variations, one might wonder which temperatures should be used as design parameters. But in literature, only a few researchers address seawater temperature variations. For instance, Giostri et al. [10] studied the off-design performance of a nominal 2.35 $MW_{net}$ plant for two scenarios using one year of 15-min-interval surface seawater temperature data in Hawaii. Hernández-Romero et al. [11] studied a solar-OTEC system considering variations in seawater temperature in Mexico. Soto & Vergara [12] showed the variations in power output based on local monthly averages of seawater temperatures in Chile from 2010. They studied an OTEC system that uses the waste heat from a neighbouring coal plant to produce electricity and freshwater. Garduño-Ruiz et al. [13] used 16 years of daily surface water temperature data to find optimal sites for OTEC in Mexico and assessed the impact of temperature variations on net power output via a temperature correlation. All these studies concluded that seawater variations have a significant impact on the plant's productivity. However, what current literature does not offer is which design approach yields the most economically feasible OTEC systems depending on inputs like local temperature profile, technical limits, and desired power output. Addressing this question is important as most designs in literature are only competitive in regions with very high electricity prices [14–16]. Hence, a design approach considering lifecycle performance could improve OTEC's economics and unlock use cases in regions where tariffs are not as high.

This paper tries to address the abovementioned knowledge gap. We developed a scalable model that sizes components for the lowest possible on-design *Levelized Cost of Electricity (LCOE)* based on the desired gross power output and constant warm and cold water temperatures that serve as design parameters. Then, the off-design analysis uses 19 years of 3-h resolution temperature data to reveal which combination of on-design warm and cold water temperature yields the lowest lifecycle LCOE. Furthermore, we present the impact of maintenance scheduling, system size, and maximum seawater pipe diameter. The model is demonstrated in detail for a 136 $MW_{gross}$ OTEC plant in Ende on Flores Island, a regency in Indonesia with a high economic potential for OTEC [17], a particularly low electrification rate [18], and a moderate electricity tariff [19]. The system size is selected to achieve a net power output of roughly 100 $MW_{net}$, which is a commonly studied

system size in OTEC literature [7,9]. To check the validity of our results outside of Ende, the model is tested with the temperature profiles from three other locations in Indonesia. For an enhanced global relevance, we also compare the LCOE with electricity tariffs from other countries suitable for OTEC.

The purpose of this research is to raise awareness of the economic impact of seawater temperature variation on the operation of an OTEC plant. Moreover, we want to show how systems can be designed to withstand off-design conditions and how their economic feasibility can be maintained. This paper contributes to OTEC research by building upon and extending existing work. Compared to Giostri et al. [10], the focus is less on the detailed engineering of the components, but more on how different design approaches and parameters affect OTEC's economics. In contrast to other studies [3,9,16,20,21], our cost assumptions do not foot on individual values but ranges, as OTEC's costs are still uncertain [1]. The use of long-term temperature data for system design is another novelty. This study also shows how OTEC can promote electrification and thus socio-economic development of disadvantaged communities with reliable, clean, and affordable baseload electricity.

The paper is structured as follows. Section 2 presents the used methods, data, equations, and assumptions. Section 3 presents and discusses the results for a 136 $MW_{gross}$ plant in Ende, Indonesia as well as the impact of aspects like system size, seasonal temperature profile, distance from plant to shore, and maximum seawater pipe diameter on the LCOE and preferred design approach. The paper ends with conclusions in Section 4.

## 2. Methods

The methodology for the scalable OTEC models consists of seven steps as illustrated in Fig. 1. In this section, each step is elaborated in detail, describing the used methods, data, equations, and assumptions.

### 2.1. Step 1: Seawater temperature data and design combinations

The first two steps encompass the download of warm and cold seawater temperature data and processing the data into a matrix with on-design temperature configurations. This study uses temperature data at 20 m and 1,000 m depth from the *HYbrid Coordinate Ocean Model (HYCOM)* for 19 years between 1994 and 2012. The metadata is listed in Table 1. Given that an OTEC plant is expected to have a useful lifetime of 30 years [7], a 30-year dataset would have been even better, but the used dataset only spans over 20 full years with the year 1993 being excluded due to too many missing data points. The coordinates refer to the coastal area at Ende, Indonesia, but the download setup can be adjusted for any other location with adequate warm and cold seawater resources. The datasets are cleaned from outliers using box and whisker plots. In this research, outliers are values that are more than 1.5 times the interquartile range away from the top or bottom of the box. The datasets are then analysed to obtain the 19-year average temperatures for each 3-h interval of the year. These average values are used to fill empty data points. To study the full 30-year lifecycle of an OTEC plant, the 19-year dataset is extended with the data from 2001 to 2011. Fig. 2 (a) shows the cleaned seawater temperature profiles at Ende for the period between 1994 and 2012.

### 2.2. Step 2: Design combinations and definition of 'bigger is better'

The designs analysed in this paper use different combinations of warm and cold seawater temperatures as design parameters. Based on the previously prepared box and whisker plots in Fig. 2(b) and Fig. 2(c), the minimum, median, and maximum warm and cold water

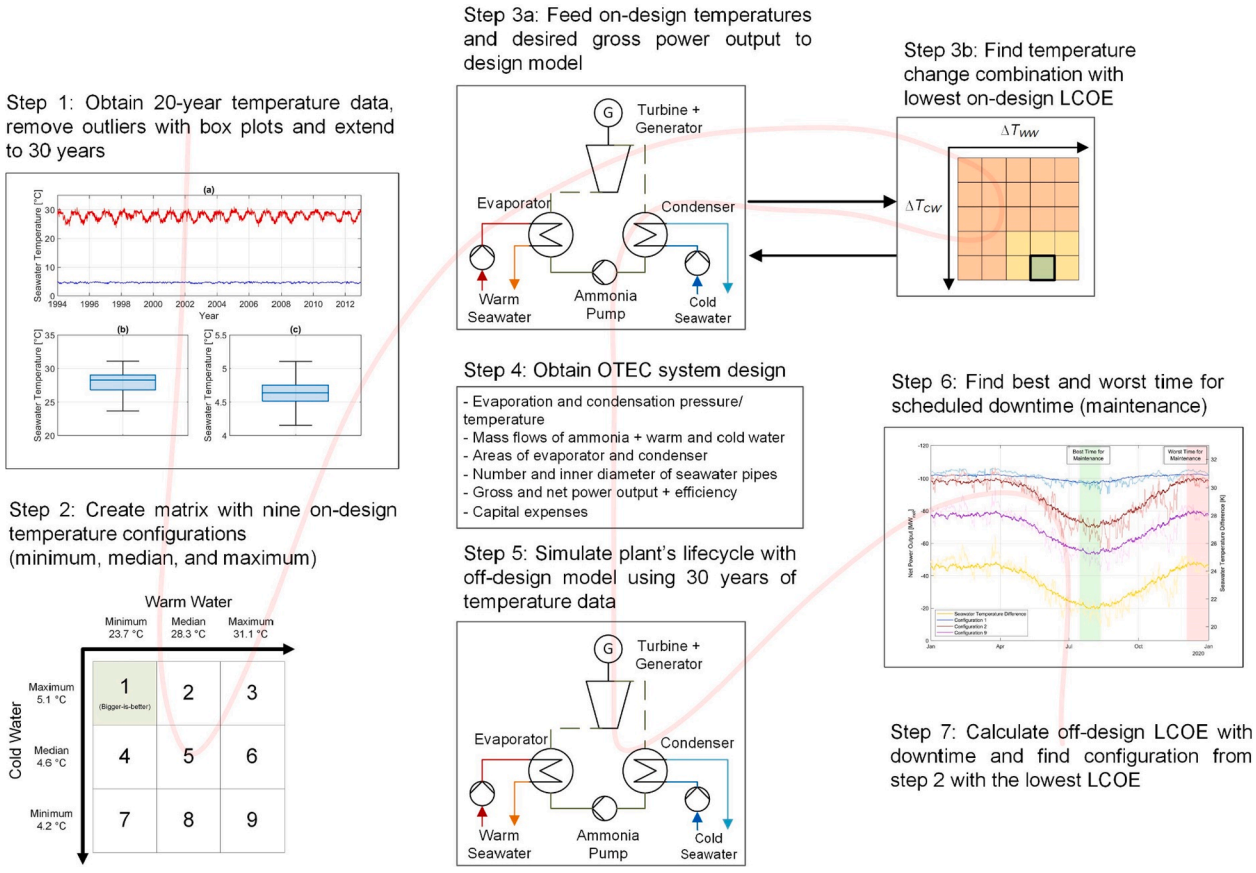


**Fig. 1.** Methodology for the scalable OTEC design model with a red line for orientation. (For interpretation of the references to colour in this figure legend, the reader is referred to the web version of this article.)

**Table 1**
Metadata of warm and cold seawater data. Coordinates refer to coastal area in Ende, Indonesia, but the coordinates can be adjusted to download temperature data for any other location worldwide with suitable ocean thermal resources.

| Title | Seawater Temperature Data |
|---|---|
| Description | Seawater temperature data at a depth of 20 m (warm water) and 1,000 m (cold water) |
| Creator | Naval Research Laboratory: Ocean Dynamics and Prediction Branch |
| Publisher | HYCOM.org |
| Dataset | GOFS 3.0: HYCOM + NCODA Global 1/12° Reanalysis/ GLBu0.08/reanalysis/ALL Data: 1992–10-02 to 2012–12-31 (3-hrly) |
| Web Link | https://ncss.hycom.org/thredds/ncss/grid/GLBu0.08/reanalysis/3hrly/dataset.html |
| Coordinate System | World Geodetic System1984 (WGS84) |
| Vertical Datum | Mean Sea Level |
| Coordinates | 121.52° E 9.04° S |
| Data Type | Point |
| Parameter Unit | °C |
| Depth Levels | 20 m and 1,000 m |
| Time Period | 01 January 1994 00:00 to 31 December 2012 21:00 |
| Temporal Resolution | 3 h |

temperatures form a total of nine *configurations*. Configuration 1 is the most conservative using the lowest warm and highest cold water temperature, while configuration 9 is the most aggressive using the highest warm and lowest cold water temperature. In this study, the term 'bigger is better' is used exclusively for configuration 1. The temperature configurations are then fed to the on-design model. Note that the model can process any thermodynamically reasonable temperature combination and is not limited to the abovementioned nine configurations.

### 2.3. Steps 3 and 4: System design and component sizing

In step 3, the user feeds the on-design warm and cold water temperatures as well as the desired gross power output to the design model. The model calculates a saturated Rankine cycle using ammonia as working fluid as follows. The liquid working fluid flows through a pump and enters the evaporator at an elevated pressure. The heat from the warm seawater is used to fully evaporate the working fluid. Next, the vapour is expanded to a lower pressure in a turbine, which drives a generator to produce electricity. The decompressed working fluid is then fully condensed with the cold seawater and transferred to the pump to complete the cycle. This study uses ammonia as a working fluid, but the model can be easily adjusted for other fluids. The model assumes an offshore OTEC plant moored to the seabed with a grid connection via an AC marine power cable. For simplicity, the only power-consuming components are seawater and ammonia pumps. With some adjustments for the cost components and the length of seawater pipes, the model could also be used for land-based systems, which is however not part of this study. All technical and economic assumptions of the model are listed in Table 2. For better readability, only key equations of the model are shown in the main text, while a complete set of equations is presented in Appendix A–B. In this research, the IUPAC convention is used, which means that heat and work flowing into the system are positive, while heat and work flowing out of the system are negative.

The values in Table 2 are based on assumptions and simplifications that are briefly discussed here. First, all efficiencies are held constant, except for the transmission efficiency, which is a function of the distance from plant to shore. Using constant efficiencies is a common practice in OTEC modelling [12,26], but one must be aware of the implications. As shown in literature [3], the efficiency of turbomachinery depends on multiple factors, like the volumetric flow of the working fluid and the design of the machine. Therefore, the power output of the turbine and power consumption of the pumps would deviate from the static values assumed here depending on the availability of ocean thermal resources and the consequent loading of the plant. Second, not all seawater and working fluid properties are computed with state functions as listed in Appendix A. Instead, the seawater and working fluid properties in Table 2 are kept constant. For the constant seawater properties, we assume a salinity of 35 $g_{Salt}/kg_{Water}$ at all studied locations and water depths. The specific heat capacity of the seawater is kept constant since

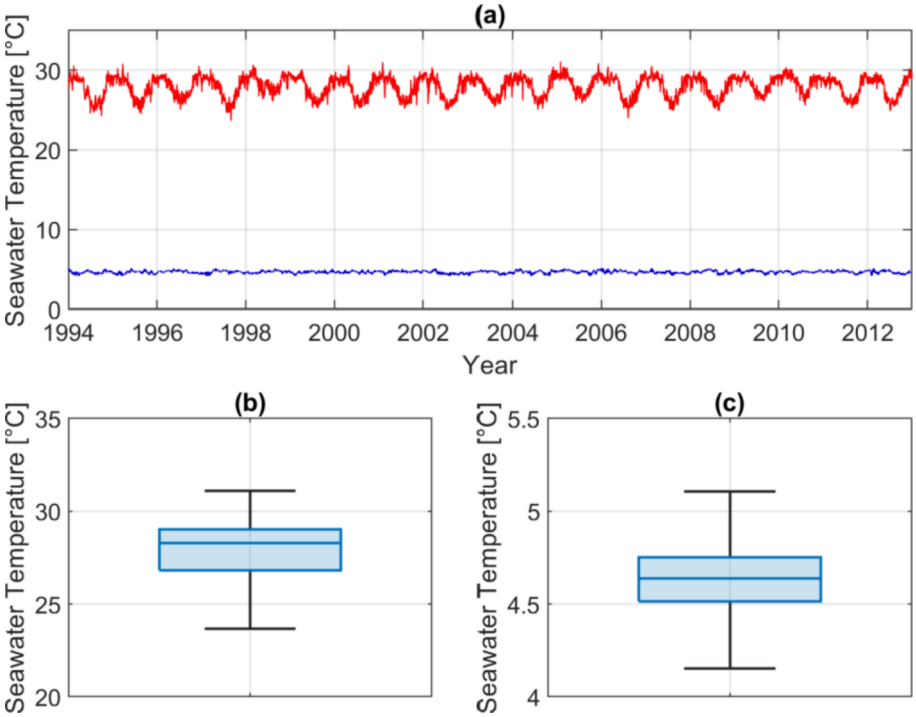


**Fig. 2.** (a) Cleaned 19-year surface and deep-sea water temperature profiles in Ende, Indonesia. Outliers are removed from the profiles using box and whisker plots for (b) surface seawater temperature and (c) deep-sea water.

**Table 2**
Technical and economic assumptions of the design model. An alternative, unformatted version of this table can be found in the dataset of this paper.

| Technical Value | Assumption [References] |
|---|---|
| **Properties Ammonia & Seawater** | |
| Density liquid ammonia $\rho_{NH3,liq}$ [kg/m$^3$] | 625 |
| Specific heat capacity seawater $c_p$ [kJ/kgK] | 4.0 [22] |
| Density surface seawater $\rho_{WW}$ [kg/m$^3$] | 1,024 [23] |
| Density deep seawater $\rho_{CW}$ [kg/m$^3$] | 1,027 [23] |
| **Heat Exchangers** | |
| Pinch-Point temperature difference evaporator and condenser $\Delta T_{pp.}$ [K] | 1.0 [24,25] |
| Nominal overall heat transfer coefficient evaporator $U_{evap,nom}$ [kW/m$^2$K] | 4.5 [3,10] |
| Nominal overall heat transfer coefficient condenser $U_{cond,nom}$ [kW/m$^2$K] | 3.5 [9,10] |
| **Turbine + Generator + Power Transmission** | |
| Isentropic efficiency turbine $\eta_{is,turb}$ [%] | 82 [26] |
| Mechanical efficiency turbine $\eta_{mech,turb}$ [%] | 95 [12,26] |
| Electrical efficiency generator $\eta_{el,gen}$ [%] | 95 [12,26] |
| **Ammonia and Seawater Pumps** | |
| Isentropic efficiency pump $\eta_{is,pump}$ [%] | 80 [10,26] |
| Electric efficiency pump $\eta_{el,pump}$ [%] | 95 [10] |
| **Seawater Pipes** | |
| Length WW pipe $l_{pipe,WW}$ [m] | 80 (20 m inlet, 60 m outlet) |
| Length CW pipe $l_{pipe,CW}$ [m] | 1,060 (1,000 m inlet, 60 m outlet) |
| Pipe thickness $t$ [m] | 0.09 [27,28] |
| Density HDPE $\rho_{HDPE}$ [kg/m$^3$] | 995 [28] |
| Density FRP-sandwich pipe $\rho_{FRP}$ [kg/m$^3$] | 1,016 [27] |
| Roughness factor $z$ [mm] | 0.0053 [26] |
| Pressure drop coefficient evaporator & condenser $K_{L,evap/cond}$ [-] | 120 |
| Nominal flow velocity in the pipes $v_{pipe,\ CW/WW}$ [m/s] | 2.0 [3,7] |
| Nominal flow velocity in the heat exchangers $v_{evap/cond,\ nom}$ [m/s] | 1.0 [3] |
| Maximum inner diameter $d_{max}$ [m] | 8 |

| Economic Value | Specific Reference Cost for Scaling | | Scale Factor $b$ [-] | | Ref Size for Scaling [MW$_{gross/pump}$] | |
|---|---|---|---|---|---|---|
| | LC | HC | LC | HC | LC | HC |
| Turbine $capex_{turb}$ [US$/kW$_{gross}$] | 328 [9] | 512 [16] | 0.16 [9,28] | | 136 | 136 |
| Heat Exchangers $capex_{HX}$ [US$/m$^2$] | 226 [16] | 916 [28] | 0.16 [23,28] | 0.09 [9,28] | 80 | 4.4 |
| Pumps $capex_{pump}$ [US$/kW$_{pump}$] | 1,674 [23] | 2,480 [23] | 0.38 [16,23] | | 5.6 | 5.6 |
| Seawater pipes $capex_{pipe}$ [US$/kg$_{pipe}$] | 9 [3,28] | 30.1 [16,27] | – | | – | – |
| Power Transmission $capex_{trans}$ [US$/kW$_{gross}$] | 10.3*$D$+68.7 [29] | 38*$D$+232.5 [17] | – | | – | – |
| Design & Management $capex_{des}$ [US$/kW$_{gross}$] | 3,113 [3] | 6,085 [28] | 0.70 [3,9] | | 4.0 | 4.4 |
| Structure & Mooring $capex_{struct}$ [US$/kW$_{gross}$] | 4,465 [23] | 7,442 [23] | 0.35 [9,23] | | 28.1 | 28.1 |
| Deployment $capex_{depl}$ [US$/kW$_{gross}$] | 650 [9] | 667 [16] | – | | – | – |
| Extra Costs $perc_{ext}$ [% of CAPEX] | 5 [28] | 20 [9] | – | | – | – |
| *OPEX* [% of CAPEX/year] | 3 [16] | 5 [9] | – | | – | – |
| **LCOE** | | | | | | |
| Project lifetime $n$ [years] | 30 [1] | | | | | |
| Discount rate *DR* [%] | 10 [17] | | | | | |
| Capacity factor $c_f$ [%] (on-design model) | 91.3 [3,30] | | | | | |

it leads to a very small error [22] and the uncertainty of local salinity. Regarding the economic assumptions in Table 2, a third limitation is that only the seawater temperature is used to design the OTEC plants. Other ocean data like salinity, metocean conditions (waves, currents, and wind) and seabed properties amongst others are omitted to limit the complexity of the designs. However, these properties affect the system's costs as it must be designed to withstand the stresses exerted by the ocean. In literature, only a few studies include a more complete set of ocean data in their techno-economic OTEC designs [9,16,28], so there would be high scientific merit if this was addressed in more detail in future research. For example, it could be shown how metocean conditions and seabed properties affect offshore structure and mooring cost. Notwithstanding the limitations above, we believe that our model still produces valuable results.

The on-design temperatures represent the inlet temperatures at the heat exchangers. During the phase-change processes of the ammonia, the temperatures of both the warm and cold seawater change. Hence, the seawater temperature differences between heat exchanger inlets and outlets are key design elements in the model, based on which all system components are sized. There are countless possible combinations of outlet temperature with varying technical and economic feasibility. To reduce the number of choices, the design model loops through warm and cold seawater temperature differences between 2 K and 5 K in 0.5 K steps, resulting in a total of 49 possible temperature difference combinations. Furthermore, the smallest temperature difference between the ammonia and seawater, or pinch-point temperature difference, is set to 1 K [24,25] for both evaporator and condenser and for all cases presented here. For example, if the outlet warm seawater temperature is 24 °C, the evaporation temperature is 23 °C. Knowing the evaporation and condensation temperatures, it is possible to obtain the respective saturation pressures, enthalpies, entropies, and exergies to calculate the thermodynamic cycle described above.

The computed mass flows of warm and cold seawater are used to size the seawater pipes. This is a crucial step, as the cold water pipe is one of the technically most challenging components of an OTEC plant. Although current state-of-the-art pipes reach inner diameters of up to 4 m [31], many OTEC studies suggest pipes with diameters of more than 10 m for large-scale plants [9,27,32,33]. Whether such pipes will ever be developed is uncertain, which is why the user can choose a maximum pipe diameter in the model. With this feature, the plant uses multiple smaller pipes instead of one large pipe. This study assumes a default maximum diameter of 8 m, which is admittedly still beyond the current state of the art, but smaller than what literature suggests. The diameters of these pipes are then calculated for a maximum seawater velocity of 2.0 m/s; in the heat exchangers, the maximum velocity is 1.0 m/s [3]. These velocities are chosen to limit both biofouling and pressure drops.

The seawater is exhausted from the system at a water depth of 60 m [27]. The pressure drops occur in our model in the seawater pipes and the heat exchangers with the equations listed in Appendix B. For the former, we use the Swamee-Jain equation to calculate the Darcy friction factor, with which the pressure drop in the pipe can be computed. For the latter, we use a constant friction factor $K_L$ as shown in Eq. (1).

$$\Delta p_{evap/cond} = \rho_{WW/CW} * \frac{v^2_{evap/cond}}{2} * K_{L,evap/cond} \quad (1)$$

With this, we want to establish a simple, direct relationship between seawater velocity in the heat exchangers $v_{evap/cond}$, seawater density $\rho$ and pressure drop $\Delta p_{evap/cond}$ without having to size the plate lengths and ports of the plate heat exchangers as done in other studies [3,10]. The friction factor $K_L$ is assumed to be constant with a value of 100 for all scenarios. This value was chosen to obtain an on-design pressure drop of 50 kPa in both evaporator and condenser at a seawater velocity in the heat exchanger channels of 1 m/s. When designing the plate heat exchangers, the number of parallel seawater channels and the plate geometry (width, length and plate spacing) can always be selected to match the 50 kPa pressure drop under on-design operating conditions. We acknowledge that the change in heat exchanger design affects the characteristics of the heat transfer performance, which is discussed in Section 2.4. If the total pressure drop in the warm or cold water system exceeds 100 kPa, the model scales down the nominal pipe and heat exchanger velocities in increments of 0.1 and 0.05 m/s, respectively, until the pressure drop is below the threshold. This feature was added for systems in the range of kW and was not needed for the systems analysed here. Moreover, we assume a constant seawater pipe thickness of 0.09 m independent of diameter and water depth. This is a simplification and we acknowledge that the pipe thickness can be optimised for these and other parameters to save pipe materials and thus costs [28].

After designing the key components of the plant, the model calculates the *Capital Expenses (CAPEX)*, *Operational Expenses (OPEX)*, and annual electricity production. Some cost components do not scale linearly with size. For some of these components, the non-linear relationship is already considered during the sizing process, as in the case of the seawater pipes. But for others, such as the offshore platform, the CAPEX must be scaled based on a reference cost and system size, as shown in Eq. (2). The inputs for Eq. (2) are deduced from existing literature where possible and divided into *low-cost (LC)* and *high-cost (HC)* assumptions. For components with no reliable scaling data, a conservative scaling factor of 0 is assumed.

$$capex = capex_0 * \left( \frac{\dot{W}_{t,gross,0}}{\dot{W}_{t,gross}} \right)^b \quad (2)$$

| Input | Index |
|---|---|
| *capex*: Specific capital expenses [US$/unit] | *0:* Reference |
| $W_{t,gross}$: Gross power output [kW] | |
| *b*: Scaling factor [-] | |

With these values, the LCOE can be computed with Eq. (3) which represents the electricity tariff required to break even with all expenses at the end of the plant's lifecycle [1]. It is useful to quantify the economic performance of a technology, especially if compared to competing technologies or the local electricity tariff. To convert future cash flows into present value, a discount rate of 10% is used [17]. All costs are converted to (2021) values using the CPI inflation calculator [34].

$$LCOE = \frac{\sum_{i=1}^{n} \frac{CAPEX_{total,i} + OPEX_i}{(1+DR)^i}}{\sum_{i=1}^{n} \frac{AEP_i}{(1+DR)^i}} \quad (3)$$

| Input | Index |
|---|---|
| *CAPEX*: Total capital expenses [US$(2021)] | *i*: Year i |
| *OPEX:* Operational expenses [US$(2021)/year] | *n:* Lifetime of OTEC plant |
| *AEP:* Annual Electricity Production [kWh/year] | |
| *DR:* Discount Rate [%] | |

The LCOE is calculated for all 49 temperature difference combinations. The model then chooses the design with the lowest LCOE and returns the corresponding system parameters, including:

- Warm and cold water temperature difference [K]
- Mass flows of ammonia, warm seawater, and cold seawater [kg/s]
- Evaporation and condensation pressures and temperatures [bar, °C]
- Heat transfer areas of evaporator and condenser [$m^2$]
- Number and diameter of seawater pipes [m]
- Net power output and net efficiency [$kW_{net}$, %]
- Capital and operational expenses [US$(2021), US$(2021)/year]

### 2.4. Step 5: Economic lifecycle analysis under off-design conditions

The on-design LCOE is only used to detect the economically most attractive design with fixed parameters. However, the on-design model does not tell whether the chosen system is economically feasible under off-design conditions. In steps 5–7, the off-design model simulates 30 years of plant operation in 3-h steps using the temperature dataset prepared in steps 1 and 2. In principal, the off-design model foots on the same equations as the on-design model with two differences. First, the off-design model uses temperature datasets instead of constant values. Hence, there are times in which available thermal resources vary from the nominal state. Second, a logic to control operational parameters is added to relevant system components to respond to the change of seawater temperatures.

An excess of thermal resources occurs if the warm seawater temperature is above or the cold seawater temperature is below the nominal temperature or both. Less water is required to evaporate/condense the same amount of ammonia. Therefore, the mass flows of seawater are reduced while the operating pressures and temperatures of the working fluid remain unchanged [7]. We chose to control the seawater mass flow in the model instead of the ammonia-related parameters to avoid unnecessary pumping of seawater and thus pump power consumption. We acknowledge the drawbacks that come with this decision, e.g. frequent load changes and consequently increased wear of equipment. Alternatively, the seawater mass flow could be held constant while controlling the ammonia mass flow directly with nozzles or bypasses. Therefore, we recommend more research on the impact of different control schemes on OTEC's economics and whether the net power output can be further increased than calculated here.

The reduction of mass flows affects several other system parameters like the heat transfer coefficient of the heat exchangers and outlet seawater temperatures. The dynamic behaviour of heat exchangers is highly complex and its full representation is beyond the scope of this paper. We simplified the change of heat transfer with a direct relationship between heat transfer coefficient and seawater mass flow as shown in Eqs. (4)–(6). With Eq. (4), we assume plate heat exchangers for both evaporator and condenser [24].

$$U_{evap/cond} = \frac{0.26 * Re^{0.65}_{evap/cond} * \mathrm{Pr}^{0.4}_{\mathrm{WW/CW}} * \left( \frac{\mu_{WW/CW}}{\mu_{W,WW/CW}} \right)^{0.14} * \lambda_{WW/CW}}{d_{evap/cond}} \quad (4)$$

$$Re_{evap/cond} = \frac{d_{evap/cond} * \rho_{WW/CW} * v_{evap/cond}}{\mu_{WW/CW}} \quad (5)$$

Assuming a constant water density $\rho$, Prandtl number $Pr$,

characteristic length of the evaporator and condenser $d_{evap/cond}$, thermal conductivity $\lambda_{WW/CW}$, and dynamic viscosity $\mu$, the new heat transfer coefficient $U_{evap/cond}$ equals:

$$U_{evap/cond} = U_{evap/cond,nom} * \left( \frac{v_{evap/cond}}{v_{evap/cond,nom}} \right)^{0.65} = U_{evap/cond,nom} * \left( \frac{\dot{m}_{WW/CW}}{\dot{m}_{WW/CW,nom}} \right)^{0.65} \quad (6)$$

Similar to Upshaw [23], this approach assumes that the seawater side heat transfer coefficient limits the overall heat transfer coefficient, which was experimentally confirmed in previous research [35,36]. This simplification is however still a limitation of our model, as other heat transfer mechanisms are neglected. Compared to the correlation established by Bernardoni et al. [3] as shown in Appendix C, which includes more heat transfer mechanisms, our correlation returns smaller heat transfer coefficients. With the consequently weaker heat transfer, this renders our results more conservative. Nonetheless, we recommend the inclusion of further heat transfer mechanisms if OTEC components should be modelled in more technical detail. The change of mass flow, outlet temperature and heat transfer coefficient are determined iteratively with Eqs. (7)–(11).

*Equations for evaporator and condenser:*

$$\dot{m}_{WW,i} = \frac{\left|\dot{Q}_{evap}\right|}{c_p * \left(T_{WW,out,i} - T_{WW,in}\right)} \qquad \dot{m}_{CW,i} = \frac{\left|\dot{Q}_{cond}\right|}{c_p * \left(T_{CW,out,i} - T_{CW,in}\right)} \quad (7)$$

$$U_{evap,i} = U_{evap,nom} * \left( \frac{\dot{m}_{WW,i}}{\dot{m}_{WW,nom}} \right)^{0.65} \qquad U_{cond,i} = U_{cond,nom} * \left( \frac{\dot{m}_{CW,i}}{\dot{m}_{CW,nom}} \right)^{0.65} \quad (8)$$

$$NTU_{evap,i} = \frac{U_{evap,i} * A_{evap}}{\dot{m}_{WW,i} * c_p} \qquad NTU_{cond,i} = \frac{U_{cond,i} * A_{cond}}{\dot{m}_{CW,i} * c_p} \quad (9)$$

$$\varepsilon_{evap,i} = 1 - e^{-NTU_{evap,i}} \qquad \varepsilon_{cond,i} = 1 - e^{-NTU_{cond,i}} \quad (10)$$

$$T_{WW,out,i+1} = T_{WW,in} - \varepsilon_{evap,i} * \left(T_{WW,in} - T_{evap}\right) \qquad T_{CW,out,i+1} = T_{CW,in} + \varepsilon_{cond,i} * \left(T_{cond} - T_{CW,in}\right) \quad (11)$$

*Repeat until:*

$$\left|T_{WW,out,i+1} - T_{WW,out,i}\right| \leq 1 * 10^{-7} \qquad \left|T_{CW,out,i+1} - T_{CW,out,i}\right| \leq 1 * 10^{-7}$$

*Under the following conditions:*

$$\dot{m}_{WW,i+1} \leq \dot{m}_{WW,nom} \qquad \dot{m}_{CW,i+1} \leq \dot{m}_{CW,nom}$$

$$U_{evap,i+1} \leq U_{evap,nom} \qquad U_{cond,i+1} \leq U_{cond,nom}$$

$$T_{WW,out,i+1} - T_{evap} \geq 1K \qquad T_{cond} - T_{CW,out,i+1} \geq 1K$$

$$\varepsilon_{evap,i+1} \leq 1 \qquad \varepsilon_{cond,i+1} \leq 1$$

A lack of thermal resources occurs if the warm seawater temperature is below or the cold seawater temperature is above the nominal temperature or both. If the cold water inlet is higher than the cold water outlet temperature prescribed by the proposed control or if the warm water inlet is lower than the warm water outlet temperature prescribed by the proposed control then the system cannot operate. Hence, the model checks the inlet seawater temperatures and adjusts the operating pressures if necessary so that the minimum temperature difference between seawater outlet and heat exchanger of 1 K is maintained. The mass flows, outlet temperatures, and heat transfer coefficients are again adjusted with Eqs. (4)–(11).

With these features, the off-design model returns operation data for 30 years in 3-h steps like gross and net power output and efficiency, mass flows, and operating pressures.

### 2.5. Steps 6 and 7: Downtime scheduling and off-design LCOE

The off-design model assumes 100% availability. Although an OTEC plant should operate as continuously as possible, downtime is sometimes unavoidable, for example for maintenance. With the 3-hourly net power output data from step 5, we detect more and less favourable periods for scheduled downtime in step 6. We assume a downtime of four consecutive weeks per year, during which the plant does not produce any electricity. This is a simplification and we acknowledge that OTEC's modular design could enable partial operation even during maintenance [16]. For a 4-week time window to be desirable, the forfeited power production should be as low as possible. To find these desirable periods, the net power output data is processed to reflect the 30-year averages at each 3-h interval in a year, similar to what is done in step 1 with the temperature data. The averaged power profile is then used to find the best and worst periods for downtime with the lowest and highest aggregated forfeited power, respectively. Next, two power production profiles are created, in which the power production is set to zero during the best and worst time windows. With these datasets, it is then possible to calculate the off-design LCOE for both good and bad maintenance scheduling. The described methodology is performed for all nine temperature configurations from step 2 to find out which design approach yields the lowest LCOE. With this model, it is possible to run hundreds of simulations with little computational effort. A limitation of this approach is that the off-design LCOE are not optimised, as no optimisation process takes place in the model. For the objectives and the scope of this paper, we believe that a simulation approach as presented here still generates valuable insights into the economic design of OTEC plants. Nonetheless, future research could assess to which extent the off-design LCOE can be further reduced with an optimisation approach.

### 2.6. Sensitivity analysis

The methodology described in this paper is demonstrated for a 136 $MW_{gross}$ OTEC plant in Ende, Indonesia. With the download setup in Table 1, the distance from plant to shore in Ende would be 22 km. Using high-resolution bathymetry data [37], it can be seen that the plant could be implemented as close as 7.8 km from shore. However, at such proximity, the HYCOM data tends to be inaccurate, which is why we used the data from the location in Table 1 and assumed a distance of 7.8 km. Although general insights can be obtained, the results are influenced by the local circumstances at Ende. Therefore, the model is tested for three other locations in Indonesia as shown in Fig. 3. The locations were not only chosen to cover all four cardinal directions of Indonesia but also to highlight the large differences in temperature profiles across regions. For example, there are large surface seawater temperature variations in Ende, while the deep-sea water is exceptionally warm in Sabang near the Indian Ocean. With these diverse cases, we can shed light on the impact of temperature profile and distance to shore on LCOE and preferred configuration. Although all four temperature profiles refer to locations in Indonesia, they could be representative of other countries as well. For example, the deep-sea water temperature profile in Sabang could be

useful in locations where deep-sea water are relatively warm, like in Florida, USA [9], while the rather stable surface seawater temperature profile in Tarakan might suit the conditions in Pacific regions like Guam [9].

Besides calculating off-design LCOE for the location-specific distances, a separate analysis is made using the distance of 7.8 km from Ende for all four cases. With this, we can observe the impact of temperature profiles and distance to shore on the LCOE separately. The temperatures, as well as the distance to shore and local electricity tariff of each location, are shown in Table 3. The 19-year profiles as well as the respective box and whisker plots are depicted in Appendix D–F. The electricity tariffs are in accordance with the current renewable energy policy scheme in Indonesia [19] and were converted to (2021) values. Moreover, the sensitivity of the maximum pipe diameter on the off-design LCOE is assessed in this paper as well.

**Table 3**
Overview of the four analysed locations. The download setup for the seawater temperature data is the same as in Table 1. An alternative, unformatted version of this table can be found in the dataset of this paper.

| | | Jayapura | Tarakan | Ende | Sabang |
|---|---|---|---|---|---|
| Coordinates OTEC plants | | 140.72° E 2.32° S | 118.4° E 3.44° N | 121.52° E 9.04° S | 95.6° E 5.84° N |
| Surface seawater temperature [°C] | Min | 27.8 | 27.5 | 23.7 | 27.0 |
| | Med | 29.2 | 28.8 | 28.3 | 28.9 |
| | Max | 30.5 | 30.0 | 31.1 | 31.0 |
| Deep-sea water temperature [°C] | Min | 4.3 | 4.0 | 4.2 | 6.1 |
| | Med | 4.6 | 4.5 | 4.6 | 6.6 |
| | Max | 4.8 | 5.2 | 5.1 | 7.1 |
| Distance to shore [km] | | 23.5 | 92.0 | 7.8 | 31.4 |
| Electricity tariff [US¢ (2021)/ kWh] | | 13.61 | 9.49 | 15.77 | 14.49 |

## 3. Results and discussion

### 3.1. Techno-economic analysis of a 136 $MW_{gross}$ plant in Ende, Indonesia

Table 4 shows the nine system designs for a 136 $MW_{gross}$ OTEC plant in Ende, Indonesia. There are significant differences in component sizes and system performance, especially between the most conservative (configuration 1) and most optimistic (configuration 9) designs. The former assumes a much lower warm seawater temperature and therefore a lower evaporation pressure. With a smaller pressure ratio in the turbine, more ammonia is needed to produce the desired gross power, which necessitates more seawater to enable the phase changes. This is in line with Martel et al. [9], where system components were sized larger with decreasing seawater temperature differences. Our designs can differ from OTEC literature as the used system parameters vary significantly across studies. For example, the ratio between warm and cold seawater mass flow ranges between 1.0 and 1.3 as shown in Table 4, while the ratio can be above 1.5 in other studies [7,9,26]. An increased warm seawater mass flow is less economical due to the higher power consumption of the seawater pumps. Instead, our model returns larger seawater temperature differences and lower mass flow ratios similar to Bernardoni et al. [3] and Giostri et al. [10]. Differences in heat exchanger areas between our and other studies can be explained by the choice of (1) heat transfer coefficients and (2) pinch-point temperature differences. Regarding (1), this study uses moderate values with 4.5 kW/$m^2$K for the evaporator and 3.5 kW/$m^2$K for the condenser. In literature, these coefficients can be up to 5.5 kW/$m^2$K [9] and 4.4 kW/$m^2$K [12], respectively. Regarding (2), we assume a relatively low pinch-point temperature difference of 1 K to reduce seawater mass flows. Nonetheless, the presented systems still fit well in current literature and the individual deviations are acceptable.

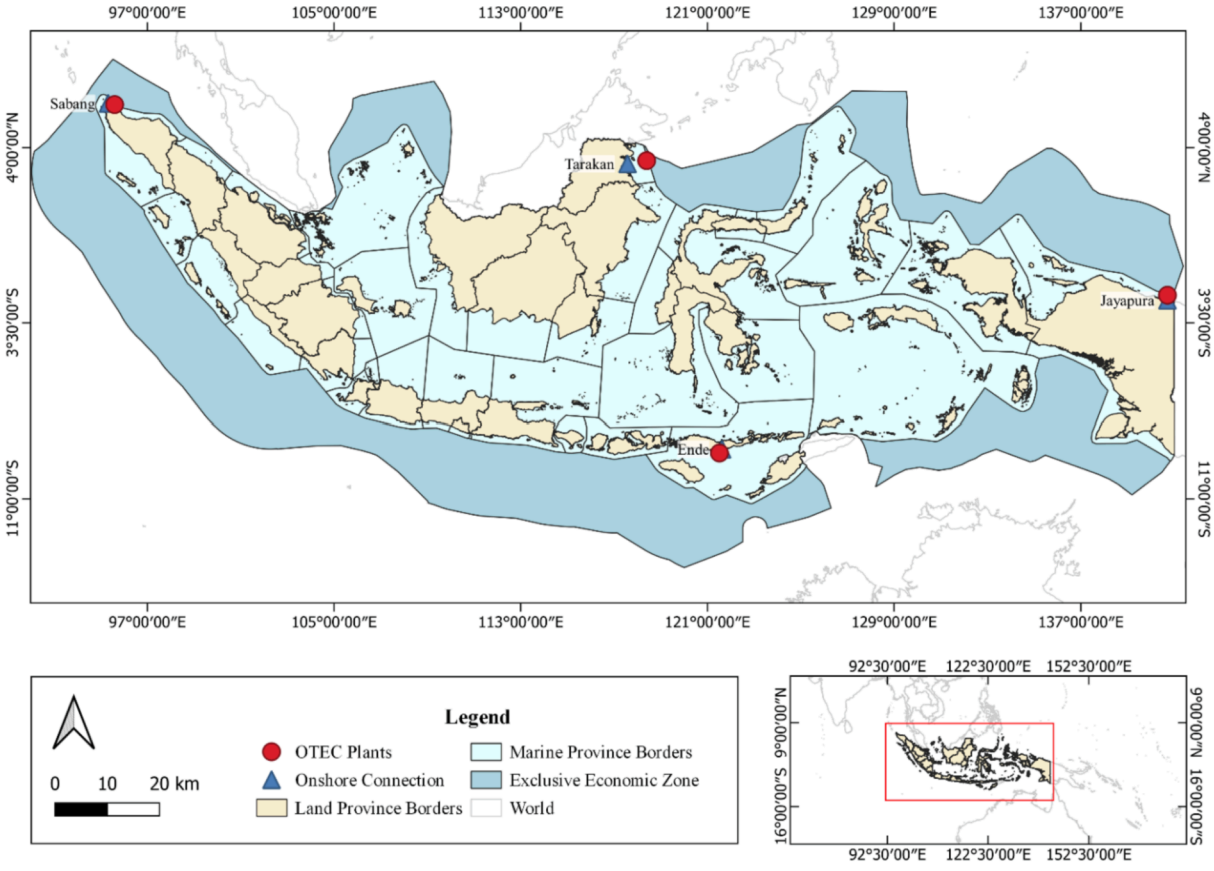


**Fig. 3.** Locations of the four seawater temperature profiles used in this study. A special focus is paid to the case in Ende as explained in the introduction.

**Table 4**
System designs for 136 $MW_{gross}$ for all nine temperature configurations and low-cost assumptions. For high-cost assumptions, only configuration 5 yielded different designs as presented in Appendix G. WW: warm water; CW: cold water. The energy and exergy balances do not always add up exactly to zero due to round-off errors.

| | **Configuration with Low-Cost Assumptions** | | | | | | | | |
|---|---|---|---|---|---|---|---|---|---|
| | **1 (Min WW+Max CW)** | **2 (Med WW+Max CW)** | **3 (Max WW+Max CW)** | **4 (Min WW+Med CW)** | **5 (Med WW+Med CW)** | **6 (Max WW+Med CW)** | **7 (Min WW+Min CW)** | **8 (Med WW+Min CW)** | **9 (Max WW+Min CW)** |
| | **Energy Balance (units in MW if not stated otherwise)** | | | | | | | | |
| Heat Evaporator | 5,551 | 4,150 | 3,506 | 4,979 | 4,143 | 3,387 | 5,020 | 4,008 | 3,298 |
| Heat Condenser | −5,417 | −4,016 | −3,372 | −4,845 | −4,009 | −3,253 | −4,886 | −3,874 | −3,164 |
| Gross Power Turbine | −136 | −136 | −136 | −136 | −136 | −136 | −136 | −136 | −136 |
| Power $NH_3$ Pump | 1.9 | 2.0 | 2.1 | 1.9 | 2.0 | 2.1 | 1.8 | 2.0 | 2.1 |
| Power WW Pump | 26.3 | 15.3 | 11.6 | 23.6 | 13.8 | 11.2 | 20.8 | 13.3 | 10.9 |
| Power CW Pump | 21.7 | 14.5 | 12.3 | 21.8 | 14.5 | 11.9 | 22.0 | 14.0 | 11.6 |
| Losses $NH_3$ Pump | 0.1 | 0.1 | 0.1 | 0.1 | 0.1 | 0.1 | 0.1 | 0.1 | 0.1 |
| Losses Turbine and Transmission | 13.5 | 13.5 | 13.5 | 13.5 | 13.5 | 13.5 | 13.5 | 13.5 | 13.5 |
| Net Power Turbine at Shore | −72.6 | −90.6 | −96.4 | −75.2 | −92.2 | −97.2 | −77.8 | −93.2 | −97.9 |
| Net Thermal Efficiency [%] | 1.3% | 2.2% | 2.8% | 1.5% | 2.2% | 2.9% | 1.5% | 2.3% | 3.0% |
| | **Exergy Balance (units in MW if not stated otherwise)** | | | | | | | | |
| Exergy Inflow Evaporator | 275 | 256 | 244 | 259 | 259 | 241 | 264 | 256 | 239 |
| Exergy Loss Evaporator | −38.1 | −35.1 | –32.5 | –33.7 | −38.1 | −31.3 | −37.8 | −36.8 | −30.4 |
| Exergy Loss Turbine | −29.5 | −29.4 | −29.4 | −29.5 | −29.4 | −29.4 | −29.5 | −29.4 | −29.4 |
| Exergy Loss Condenser | −73.0 | −57.4 | −48.2 | −61.7 | −57.6 | −46.7 | −62.5 | −55.9 | −45.6 |
| Exergy Loss $NH_3$ Pump | −0.1 | −0.1 | −0.1 | −0.1 | −0.1 | −0.1 | −0.1 | −0.1 | −0.1 |
| Exergy Loss WW Pump | −26.3 | −15.3 | −11.6 | –23.6 | −13.8 | −11.2 | −20.8 | −13.3 | −10.9 |
| Exergy Loss CW Pump | −21.7 | −14.5 | −12.3 | −21.8 | −14.5 | −11.9 | –22.0 | −14.0 | −11.6 |
| Exergy Loss Conversion Losses | −13.5 | −13.5 | −13.5 | −13.5 | −13.5 | −13.5 | −13.5 | −13.5 | −13.5 |
| Exergy Outflow at Shore | −72.6 | −90.6 | −96.4 | −75.2 | −92.2 | −97.2 | −77.8 | −93.2 | −97.9 |
| Net Exergy Efficiency [%] | 26.4% | 35.4% | 39.5% | 29.0% | 35.6% | 40.3% | 29.5% | 36.4% | 40.9% |
| Carnot Efficiency [%] | 4.9% | 6.2% | 7.0% | 5.2% | 6.2% | 7.1% | 5.3% | 6.4% | 7.3% |
| Second Law Efficiency [%] | 26.4% | 35.4% | 39.5% | 29.0% | 35.6% | 40.3% | 29.5% | 36.4% | 40.9% |
| | **Mass Flows** | | | | | | | | |
| Mass Flow $NH_3$ [kg/s] | 4,523 | 3,379 | 2,850 | 4,043 | 3,368 | 2,749 | 4,073 | 3,254 | 2,673 |
| Mass Flow WW [kg/s] | 396,531 | 230,564 | 175,284 | 355,627 | 207,150 | 169,357 | 313,781 | 200,403 | 164,899 |
| Mass Flow CW [kg/s] | 300,962 | 200,808 | 168,589 | 302,789 | 200,449 | 162,661 | 305,395 | 193,702 | 158,202 |
| | **Temperature Changes** | | | | | | | | |
| Temperature Change WW [K] | 3.5 | 4.5 | 5.0 | 3.5 | 5.0 | 5.0 | 4.0 | 5.0 | 5.0 |
| Temperature Change CW [K] | 4.5 | 5.0 | 5.0 | 4.0 | 5.0 | 5.0 | 4.0 | 5.0 | 5.0 |
| | **Evaporator and Condenser** | | | | | | | | |
| Area Evaporator [$m^2$] | 530,146 | 349,381 | 279,171 | 475,458 | 329,923 | 269,730 | 448,899 | 319,177 | 262,630 |
| Evaporation Temperature [°C] | 19.2 | 22.8 | 25.1 | 19.2 | 22.3 | 25.1 | 18.7 | 22.3 | 25.1 |
| Evaporation Pressure [bar] | 8.4 | 9.4 | 10.1 | 8.4 | 9.2 | 10.1 | 8.2 | 9.2 | 10.1 |
| Area Condenser [$m^2$] | 586,360 | 411,201 | 345,223 | 556,938 | 410,465 | 333,084 | 561,731 | 396,648 | 323,954 |
| Condensation Temperature [°C] | 10.6 | 11.1 | 11.1 | 9.6 | 10.6 | 10.6 | 9.2 | 10.2 | 10.2 |
| | 6.3 | 6.4 | 6.4 | 6.1 | 6.3 | 6.3 | 6.0 | 6.2 | 6.2 |

(*continued on next page*)

**Table 4** (*continued*)

| | Configuration with Low-Cost Assumptions | | | | | | | | |
|---|---|---|---|---|---|---|---|---|---|
| | **1 (Min WW+Max CW)** | **2 (Med WW+Max CW)** | **3 (Max WW+Max CW)** | **4 (Min WW+Med CW)** | **5 (Med WW+Med CW)** | **6 (Max WW+Med CW)** | **7 (Min WW+Min CW)** | **8 (Med WW+Min CW)** | **9 (Max WW+Min CW)** |
| Condensation Pressure [bar] | | | | | | | | | |
| | **Seawater Pipes** | | | | | | | | |
| Diameter CW Pipes [m] | 7.9 | 7.9 | 7.2 | 7.9 | 7.9 | 7.1 | 7.9 | 7.7 | 7.0 |
| Number of CW Pipes | 6 | 4 | 4 | 6 | 4 | 4 | 6 | 4 | 4 |
| Diameter WW Pipes [m] | 7.9 | 6.9 | 7.4 | 7.4 | 6.6 | 7.3 | 7.0 | 7.9 | 7.2 |
| Number of WW Pipes | 8 | 6 | 4 | 8 | 6 | 4 | 8 | 4 | 4 |

From Table 4, it seems that system components should be maximally downsized, as net power output, net thermal efficiency and net exergy efficiency are the highest for the less-is-more approach of configuration 9. In contrast, configuration 1 has the lowest on-design performance, which is especially apparent for the cold-water side of the system, where the cold-water pump and condenser are responsible for half of the systems exergy loss. However, the tables turn once the systems are exposed to off-design conditions as shown in Fig. 4. The direct relationship between seawater temperature and net power output becomes clear for all configurations. But while the short-term and seasonal variations of power output are small for the conservative design, the variations are much stronger for configurations 2 and 9. Furthermore, the power output gap between configurations 2 and 9 demonstrates a season-independent deterioration of performance with downsizing. This is because the high nominal seawater temperature and corresponding net power output of the optimistic system only occur occasionally. For configuration 9, the targeted net power output of 100 $MW_{net}$ was only reached once in 30 years, as shown in the light purple power profile in Fig. 4. Hence, a 'bigger-is-better' design approach is preferable if one of OTEC's biggest benefits should be maximised, namely its continuous, reliable baseload character. We want to point out though that OTEC's power output variations are far more predictable and manageable than the intraday variations from solar PV and wind power.

Fig. 4 also underlines the impact of downtime for maintenance. The difference of forfeited power production, illustrated with the green and red areas, is rather small for configuration 1 and increases with downsizing. Therefore, 'bigger-is-better' not only provides more flexibility when scheduling maintenance but also more resilience in case of unscheduled downtime, e.g. due to malfunction. This insight might be valuable for upcoming OTEC pilots, as operational experience is still limited today and any unplanned downtime could influence how the success of the projects is perceived.

Fig. 4 highlights that bigger components are better if the focus lies on continuity of power production, but at what cost does this benefit come? As Table 5(a) shows, costs vary considerably across configurations by 21–32%. The differences in net power output are even higher, as configuration 1 generates 44–48% more electricity throughout its lifetime than configuration 9 in Table 5(b). In terms of LCOE however, 'bigger-is-better' does not yield the lowest LCOE, but configuration 2 which uses the median warm water temperature as a design parameter. This is explained by the large surface seawater variations in Ende throughout the year, which makes it more costly to size the plant for

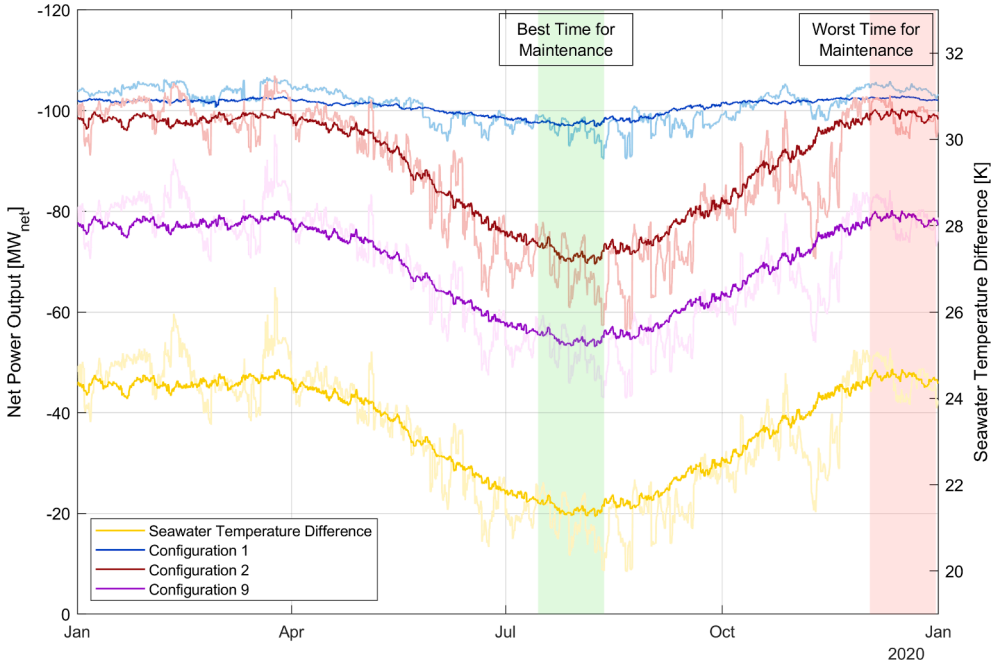


**Fig. 4.** Profiles of net power output and seawater temperature difference for three system configurations. Dark lines: Averaged values over 30 years. Light lines: Values from the year with maximum power production. Green and red areas show the best and worst times for maintenance based on averaged power profiles, respectively. (For interpretation of the references to colour in this figure legend, the reader is referred to the web version of this article.)

worst-case thermal resources. Table 5 also shows that a too optimistic design approach is not only technically, but also economically less favourable. Any configurations using the maximum warm water temperature return significantly higher LCOE compared to the rest. This does not change even if downtime scheduling is considered in Table 5(d) where poor maintenance timing can deteriorate the LCOE by up to 3%. This might not seem like much, but if downtime occurs at the worst possible times, the impact of bad downtime scheduling can be high enough to render configuration 1 the most economic for low-cost assumptions. Therefore, this underlines again that a 'bigger-is-better' design approach increases the plant's economic resilience against sub-optimally planned maintenance or unscheduled downtime.

Assuming well-planned maintenance, Fig. 5 shows the cash flows of the economically best low-cost and high-cost plants against the local electricity tariff of 15.77 US¢(2021)/kWh in Ende. The low-cost plant breaks even after roughly 24 years with a net present value of 44 US$ million after 30 years. This is lower than the previously studied 100 $MW_{net}$ OTEC plant in Buru Island, Indonesia, where the electricity tariff is higher [17]. Nonetheless, we show that an off-design analysis is helpful to obtain economically feasible system designs, as only three of the nine low-cost configurations in Table 5 yield an LCOE below the current tariff. As in our earlier work, the high-cost plant does not reach a positive net present value [17]. Nonetheless, most of these high costs are expected to stem from OTEC's early development stage and should only occur in first-of-its-kind projects. With more experience gathered during commercialisation, the costs should move more towards the low-cost range and maybe even below that [2].

### 3.2. The impact of system size and cost assumptions

So far, our results only refer to the system size of 136 $MW_{gross}$. But given the small size of current pilot plants, OTEC must still be significantly scaled up to materialise the economic opportunities discussed above. Therefore, the model is tested and validated for small-scale, medium-scale, and large-scale systems of 4.4 [3,10,28], 80 [16,27], and 136 $MW_{gross}$ [7,9,17], respectively. The costs calculated here are compared to two previously created cost scale curves based on recent literature. These curves reflect two possible levels of OTEC costs, namely a high-cost curve by Lockheed Martin [9,28] and a low-cost curve by Vega [7]. A third cost curve with even lower costs is omitted here since the underlying system designs and cost assumptions have not been validated yet [1]. As depicted in Fig. 6, the range of costs in this study are mostly in line with literature except for the 4.4 $MW_{gross}$ system. This is because we extracted the component costs from several studies and used the lowest and highest values as our cost range. Therefore, the scale factors and cost assumptions between our, Lockheed Martin's [9,28], and Vega's [7,16,38] work can differ to a varying extent. For example, although Vega's [7,16] total system costs are lower than Lockheed Martin's [9,28], the former calculated markedly higher seawater pipe costs. For the pipes, Vega [16,38] assumes a sandwich construction with two *fibre-reinforced plastic (FRP)* sheets separated by a layer of syntactic foam as pipe material, while Lockheed Martin uses HDPE for small [28] and FRP for large systems [9]. In contrast, we take HDPE pipes for all low-cost and FRP-sandwich construction pipes for all high-cost systems at any system size. The impact of these assumptions are less severe for larger systems, which is why the deviations are not as large. Moreover, we use values from the offshore wind industry [29] for the lower end of

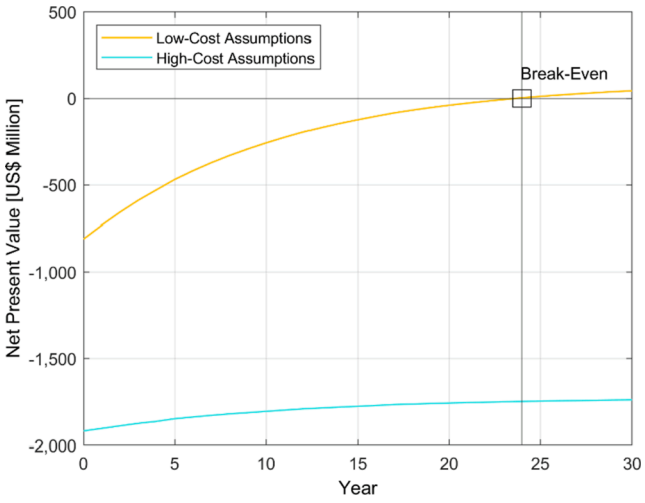


**Fig. 5.** Cash flow diagrams for a 136 $MW_{gross}$ plant in Ende under low-cost and high-cost assumptions.

**Table 5**
Key results from the techno-economic analysis of a 136 $MW_{gross}$ OTEC plant in Ende, Indonesia with (a) total capital expenses, (b) lifecycle electricity production, and LCOE with (c) well and (d) poorly timed maintenance. An alternative, unformatted version of this table can be found in the dataset of this paper.

| **(a) LC-CAPEX [US$ million]** | | **Warm Water** | | | **HC-CAPEX [US$ million]** | | **Warm Water** | | |
|---|---|---|---|---|---|---|---|---|---|
| | | *Min* | *Med* | *Max* | | | *Min* | *Med* | *Max* |
| **Cold Water** | *Max* | 921 | 810 | 772 | **Cold Water** | *Max* | 2,314 | 1,918 | 1,784 |
| | *Med* | 902 | 804 | 766 | | *Med* | 2,244 | 1,888 | 1,762 |
| | *Min* | 895 | 797 | 761 | | *Min* | 2,224 | 1,872 | 1,747 |
| **(b) LC-/ HC Lifecycle Electricity Production Good O&M [TWh]** | | **Warm Water** | | | **LC-/ HC Lifecycle Electricity Production Bad O&M [TWh]** | | **Warm Water** | | |
| | | *Min* | *Med* | *Max* | | | *Min* | *Med* | *Max* |
| **Cold Water** | *Max* | 24.6 | 22.0 | 17.9 | **Cold Water** | *Max* | 24.5 | 21.4 | 17.4 |
| | *Med* | 23.3 | 21.3/ 21.4 | 17.6 | | *Med* | 23.2 | 20.8/ 20.9 | 17.1 |
| | *Min* | 21.9 | 20.6 | 17.1 | | *Min* | 21.8 | 20.2 | 16.6 |
| **(c) LC-LCOE Good Downtime [US¢/kWh]** | | **Warm Water** | | | **HC-LCOE Good Downtime [US¢/kWh]** | | **Warm Water** | | |
| | | *Min* | *Med* | *Max* | | | *Min* | *Med* | *Max* |
| **Cold Water** | *Max* | 15.33 | 15.12 | 17.65 | **Cold Water** | *Max* | 44.16 | 41.09 | 46.81 |
| | *Med* | 15.83 | 15.46 | 17.86 | | *Med* | 45.21 | 41.52 | 47.15 |
| | *Min* | 16.70 | 15.84 | 18.24 | | *Min* | 47.58 | 42.69 | 48.00 |
| **(d) LC-LCOE Bad Downtime [US¢/kWh]** | | **Warm Water** | | | **HC-LCOE Bad Downtime [US¢/kWh]** | | **Warm Water** | | |
| | | *Min* | *Med* | *Max* | | | *Min* | *Med* | *Max* |
| **Cold Water** | *Max* | 15.39 | 15.52 | 18.19 | **Cold Water** | *Max* | 44.35 | 42.17 | 48.20 |
| | *Med* | 15.90 | 15.86 | 18.38 | | *Med* | 45.41 | 42.59 | 48.53 |
| | *Min* | 16.77 | 16.25 | 18.77 | | *Min* | 47.79 | 43.81 | 49.41 |

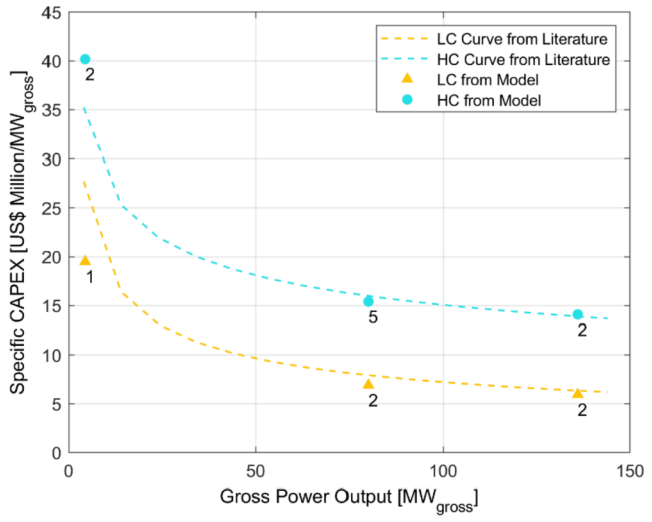


**Fig. 6.** Comparison of specific CAPEX from the model with values from literature [1]. The original scale curves were adjusted from nominal net to gross power output for better comparison. The labels next to the data points show the chosen temperature configurations.

power transmission costs, as these are far lower than the ones from OTEC literature [9,16]. From Fig. 6, it can be seen that only the low-cost 4.4 $MW_{gross}$ system would be designed according to 'bigger-is-better'. As no clear trend of selected configuration can be seen for both cost assumptions, this shows that it may be wise to find the most economic configuration on a case-to-case basis.

Table 6 breaks down the costs calculated in this study. Most component costs fit well with the estimations found in literature, with deviations in structure and mooring, pipe, pump, and turbine costs originating mostly from the mixed use of cost assumptions from different studies. For low-cost OTEC, deviations from literature occur due to the addition of cost components that were not included in the original studies, e.g. design and management costs as well as extra costs for permits, auxiliary systems, and contingencies amongst others.

From what we have shown so far, the high-cost range is not very desirable. Therefore, we present three recommendations on how the high-cost arrangement could be avoided or costs could be reduced towards the low-cost range. First, technological advances must either enable HDPE pipes with diameters beyond 4 m or drive down the cost of FRP-sandwich pipes by factor 2–3. Pipe costs can have an enormous impact on OTEC's economic performance, so a low-cost pipe with sufficient structural integrity is needed for OTEC to thrive [16,28]. However, it is unclear whether HDPE pipes can be scaled up for larger systems, as HDPE is not as structurally stable as FRP and state-of-the-art pipes have not reached the required diameters yet. But in contrast to OTEC literature [7,9,32], we do not think that pipe diameters beyond 8 m are necessary to make OTEC economically feasible. So, the technology gap might not be as big as suggested by literature. Second, the most uncertain costs revolve around structure and mooring and limiting them without abandoning operational safety is essential. This could be done by first focussing on small land-based systems without an offshore structure, followed by a careful roll-out of gradually larger plants nearshore in idle waters. Increased costs due to longer seawater pipes and larger seawater pumps could be compensated by a less complex installation of the seawater pipes along the seabed, as OTEC developers could benefit from current experience in marine pipeline laying. With sufficient operational experience, full-scale systems could be deployed further off-shore in rougher waters. Third, the establishment of a clear regulatory groundwork for OTEC deployment is important to limit project management and administration cost. Depending on the country and its legal structure, an OTEC plant could be under the responsibility of several ministries. Without an appropriate legal framework, there is the risk of unclear responsibilities and misaligned interests which might cause unnecessary delays and costs. To convince policy makers to lay the regulatory groundwork, a stronger case for OTEC must be built. The first step towards this could be to directly address current technical barriers, e.g. regarding offshore structure, mooring, and seawater pipes. Moreover, it could be beneficial to create a global map of economically

**Table 6**
Cost breakdown for different system sizes of (a) low-cost and (b) high-cost OTEC in Ende. An alternative, unformatted version of this table can be found in the dataset of this paper.

| **(a) Low-Cost OTEC** | **Absolute Cost [US$(2021) Thousand] / Specific Cost [US$(2021)/Unit] / Relative Cost [%]** | | | | | | | | |
|---|---|---|---|---|---|---|---|---|---|
| **Component** | **4.4 $MW_{gross}$** | | | **80 $MW_{gross}$** | | | **136 $MW_{gross}$** | | |
| Turbine + Generator | 2,499 | 568 US$/kW$_{gross}$ | 3% | 28,565 | 357 US$/kW$_{gross}$ | 5% | 44,608 | 328 US$/kW$_{gross}$ | 6% |
| Evaporator | 4,006 | 359 US$/m$^2$ | 5% | 46,447 | 226 US$/m$^2$ | 8% | 72,533 | 208 US$/m$^2$ | 9% |
| Condenser | 4,990 | | 6% | 54,665 | | 10% | 85,367 | | 11% |
| Pumps | 3,653 | 2,983 US$/kW$_{pump}$ | 5% | 20,035 | 1,051 US$/kW$_{pump}$ | 4% | 27,570 | 864 US$/kW$_{pump}$ | 3% |
| Seawater Pipes | 6,184 | 9 US$/kg | 8% | 35,629 | 9 US$/kg | 6% | 47,085 | 9 US$/kg | 6% |
| Power Transmission | 655 | 19 US$/kW/km | 1% | 11,915 | 19 US$/kW/km | 2% | 20,256 | 19 US$/kW/km | 3% |
| Structure + Mooring | 37,594 | 8,544 US$/kW$_{gross}$ | 48% | 247,672 | 3,096 US$/kW$_{gross}$ | 45% | 349,678 | 2,571 US$/kW$_{gross}$ | 43% |
| Design + Management | 12,723 | 2,892 US$/kW$_{gross}$ | 16% | 30,373 | 380 US$/kW$_{gross}$ | 5% | 35,615 | 262 US$/kW$_{gross}$ | 4% |
| Installation | 2,860 | 650 US$/kW$_{gross}$ | 4% | 52,000 | 650 US$/kW$_{gross}$ | 9% | 88,400 | 650 US$/kW$_{gross}$ | 11% |
| Extra Cost | 3,758 | 854 US$/kW$_{gross}$ | 5% | 26,365 | 330 US$/kW$_{gross}$ | 5% | 38,556 | 283.5 US$/kW$_{gross}$ | 5% |
| Total CAPEX | 78,922 | | | 553,667 | | | 809,668 | | |
| OPEX | 2,368 | | | 16,610 | | | 24,290 | | |
| **(b) High-Cost OTEC** | **Absolute Cost [US$(2021) Thousand] / Specific Cost [US$(2021)/Unit] / Relative Cost [%]** | | | | | | | | |
| **Component** | **4.4 $MW_{gross}$** | | | **80 $MW_{gross}$** | | | **136 $MW_{gross}$** | | |
| Turbine + Generator | 3,901 | 887 US$/ kW$_{gross}$ | 2% | 44,589 | 557 US$/ kW$_{gross}$ | 3% | 69,632 | 512 US$/ kW$_{gross}$ | 4% |
| Evaporator | 10,354 | 916 US$/m$^2$ | 6% | 143,747 | 699 US$/m$^2$ | 11% | 232,604 | 666 US$/m$^2$ | 12% |
| Condenser | 12,186 | | 7% | 169,182 | | 13% | 273,761 | | 14% |
| Pumps | 5,436 | 4,407 US$/kW$_{pump}$ | 3% | 29,681 | 1,557 US$/kW$_{pump}$ | 2% | 40,844 | 1,280 US$/kW$_{pump}$ | 2% |
| Seawater Pipes | 20,770 | 30.1 US$/kg | 12% | 121,673 | 30.1 US$/kg | 9% | 160,798 | 30.1 US$/kg | 8% |
| Power Transmission | 2,328 | 68 US$/kW/km | 1% | 42,319 | 68 US$/kW/km | 3% | 71,942 | 68 US$/kW/km | 4% |
| Structure + Mooring | 62,659 | 12,241 US$/kW$_{gross}$ | 35% | 412,805 | 5,161 US$/kW$_{gross}$ | 32% | 582,824 | 4,285 US$/kW$_{gross}$ | 30% |
| Design + Management | 26,774 | 6,085 US$/kW$_{gross}$ | 15% | 63,915 | 799 US$/kW$_{gross}$ | 5% | 74,944 | 551 US$/kW$_{gross}$ | 4% |
| Installation | 2,935 | 667 US$/kW$_{gross}$ | 2% | 53,360 | 667 US$/kW$_{gross}$ | 4% | 90,712 | 667 US$/kW$_{gross}$ | 5% |
| Extra Cost | 29,468 | 6,697 US$/kW$_{gross}$ | 17% | 216,254 | 2,703 US$/kW$_{gross}$ | 17% | 319,612 | 2,350 US$/kW$_{gross}$ | 17% |
| Total CAPEX | 176,811 | | | 1,297,527 | | | 1,917,673 | | |
| OPEX | 8,841 | | | 64,876 | | | 95,884 | | |

promising locations for OTEC.

### 3.3. Impact of the maximum inner diameter of seawater pipes

The seawater pipe is a complex component and caused the failure of previous OTEC projects as in the case of the 1 MW floating OTEC plant that was planned in India in 2000 [4]. It would be tempting to use smaller, technically more feasible pipes. However, the technical feasibility must be balanced with the plant's economics. Smaller pipes increase the pump power consumption and the specific pipe costs due to reduced economies of scale. Therefore, this section assesses the impact of maximum inner pipe diameter on the LCOE and preferred temperature configuration. OTEC literature uniformly proposes large pipes for large-scale systems [9,27,32,33], so this section offers an alternative.

Fig. 7 shows a strong, non-linear impact of maximum pipe diameter on the LCOE. With a diameter of 2 m, over 146 pipes with a total length of 35 km would be needed for a 136 $MW_{gross}$ plant. These pipes would probably require a large floating vessel and wake effects at the deep end of the pipes might curb the extraction of cold seawater. Both these impacts are not considered in our model, which is why the techno-economic infeasibility of a 2 m diameter pipe might not be fully reflected here. A pipe diameter of 5.5 m already shows much improvement and only 20 pipes with a total length of about 5 km are needed. These pipes could fit on platforms currently studied in literature [27,32,39] and wake effects should be less severe. Based on the electricity tariff in Ende, a low-cost plant with 5.5 m pipes would already be economic. This is an interesting finding, as OTEC could be economically attractive with pipe diameters that are much smaller than the ones suggested in other studies [9,27,32,33].

In terms of maximum pipe diameter, the LCOE can only be improved until one inlet and outlet pipe can each convey the required amount of seawater. For the cold water pipe, this occurs at diameters of 12.5 m. In the case of low-cost OTEC, using a diameter of 16 m instead of 9 m improves the LCOE merely by 2%, so the added value of such a large pipe is contestable. Regardless of maximum pipe diameter and cost assumptions, configuration 2 is preferred in Ende.

Note that these observations only apply for a depth of 1,000 m, which was chosen due to its prominence in literature [3,7,28]. However, as listed by Vera et al. [26], a 31.5 kW OTEC plant that operated in Nauru in 1981 extracted sufficiently cold seawater from depths of 500–700 m. Shortening the cold seawater pipe entails a trade-off between lower pipe costs on the one hand and lower power production on the other hand, as the deep-sea water is warmer at shallower depths. Our model does not consider this trade-off, so we recommend the validation of this section's results for different water depths. Soto and Vergara [12] already studied the economic impact of the water depth, but only for the specific evaporator and condenser plate costs as well as cold water pipeline costs, but not for the entire system costs. A way to assess the impact of water depth on system costs could be to add a feature to our model that techno-economically optimises the seawater pipe length based on off-design conditions.

### 3.4. Impact of local seawater temperature profile

Fig. 8 shows for the four locations introduced in Section 2.6 how different temperature profiles and distances to shore affect the off-design LCOE and system configuration for a 136 $MW_{gross}$ system. It can be seen that not only a high magnitude of thermal resource is important when choosing an OTEC site, but also a minimal seasonal variation, as a low temperature variation means a low deviation from the design temperatures. Using a uniform distance of 7.8 km, the lowest LCOE are in Jayapura and Tarakan, where the surface seawater and deep-sea water temperature variations are the lowest. The highest distance-adjusted LCOE is found in Sabang, where the deep seawater temperature is by far the highest among the four sites. Moreover, Fig. 8 reveals that favourable thermal resources can be nullified if the plant is located too far from shore. For location-specific distances, the plant in Tarawan yields the highest LCOE, although the thermal resources there are the second best after Jayapura. The plant would be situated more than 90 km away from shore and the resulting surplus cable costs and transmission losses render the plant in Tarawan uneconomic.

Regarding the configuration, Ende is the only location where configuration 2 was preferred over configuration 1. This underlines our hypothesis from Section 3.1 where we stated that the high seasonal temperature variation of the surface seawater increases the costs for sizing the system for worst-case thermal resources. Therefore, it can be deduced that 'bigger-is-better' applies in locations where surface seawater temperature variations are low to moderate. For locations with high variations, it is economically more favourable to opt for median surface seawater temperatures as design parameters.

It might be sobering that Ende is the only case in Fig. 8 where the LCOE is below the local electricity tariff. This is not only due to OTEC's current economic challenges, but also due to the nature of Indonesia's energy policies as discussed in earlier studies [2,17]. With more supportive policies, OTEC's unique set of benefits could come into play.

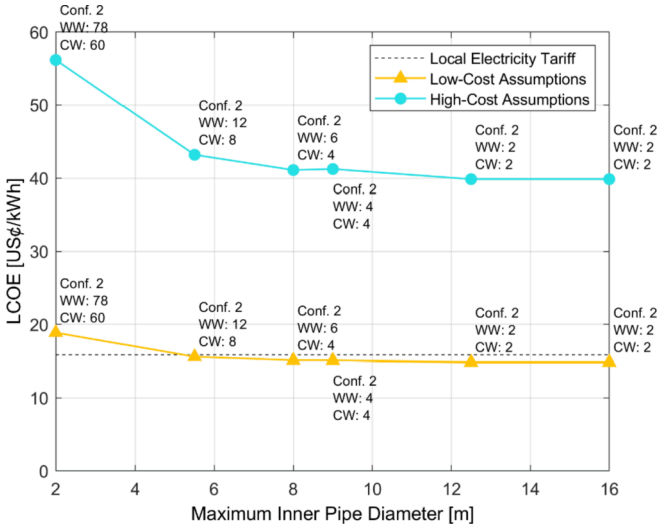


**Fig. 7.** Impact of maximum seawater pipe diameter on the LCOE at 136 $MW_{gross}$. Labels show temperature configurations and the number of required pipes.

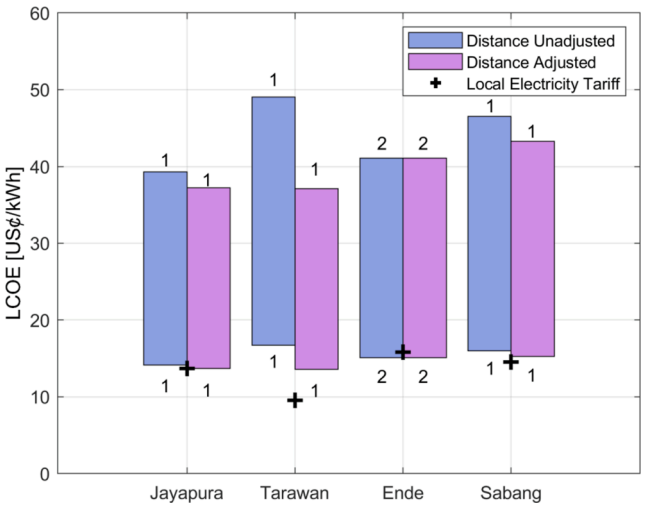


**Fig. 8.** Impact of seawater temperature profiles and distance to shore on the LCOE range for a 136 $MW_{gross}$ system. The labels show the temperature configuration with the lowest LCOE.

With a carbon tax, for example, clean OTEC power could become more cost-competitive against fossil fuel-powered baseloads like coal. If the social acceptance of the energy transition is to be fostered by limitations on land use, offshore OTEC could have a competitive edge against land-area-intense technologies like solar PV, onshore wind, geothermal, and hydropower. Therefore, Fig. 8 should be seen as a snapshot under current energy policies without taking into account OTEC's economic potential under a more favourable policy landscape.

But what about other countries? If we compare the location-specific range of LCOE from Tarakan to the global electricity tariffs reported in Seungtaek et al. [15], we see that a profitable operation could be feasible in the USA (Hawaii), Brazil (Fernando de Noronha), Australia (Rainbow Beach), the Philippines (Manay), Kiribati (Tarawa), Japan (Kumejima), Samoa (Ofu), Nigeria (Lagos), Kenya (Lamu), Gabon (Port Gentil), and Jamaica (Montego). Of course, it would have to be assessed in more detail whether there is an actual demand for a 136 $MW_{gross}$ plant in these locations, and the respective temperature profiles might differ from the ones in Tarakan, which affects the local LCOE. Nonetheless, we demonstrate that OTEC is not only interesting in Indonesia, but countries all over the world and we hope this paper encourages researchers to look deeper into global OTEC's economic feasibility.

Fig. 8 underlines once more how important a good understanding of the local thermal resources is when designing an OTEC plant. One might wonder to which extent the temperature data from HYCOM is suitable to obtain such understanding, especially at near-shore locations. A limited accuracy near shore is not a limitation of HYCOM specifically, but of many other ocean models and specialised software is necessary to capture the complex near-shore behaviour of the ocean [40,41]. This is a dilemma since OTEC's economic potential depends on a close distance to shore [17]. An alternative to HYCOM would be to collect data with field measurements. However, the increased reliability of temperature data with measurements currently comes at a high cost. Not many companies have the necessary equipment and expertise to conduct deep-sea measurements at the required accuracy. Therefore, collecting long-term field data may be more adequate at advanced project phases. Until then, HYCOM offers one of the most valuable sources for global temperature data and the abovementioned limitation is acceptable.

## 4. Conclusion

This paper sheds light on which design approach yields the most economic *Ocean Thermal Energy Conversion (OTEC)* system in terms of *Levelized Cost of Electricity (LCOE)* considering off-design conditions. We used different combinations of warm and cold seawater temperatures to design OTEC systems and compared their economic long-term performance using 19 years of 3-hourly temperature data. OTEC is a technology that is most economic at large system sizes and we found that the credo 'bigger is better' also has benefits if applied to the component level. 'Bigger-is-better' systems are sized based on worst-case ocean thermal resources and among the studied system designs, their power output was by far the largest and most continuous. Therefore, 'bigger-is-better' systems emphasise one of OTEC's strongest benefits, namely its predictable baseload generation. Furthermore, 'bigger-is-better' increases the economic resilience against sub-optimally planned or unexpected downtime, which might be important to curb investment risks. These benefits aside, we also found that 'bigger-is-better' systems are more expensive than less conservatively designed systems. In locations where seasonal seawater temperature variations are low or moderate, these surplus costs can be compensated by a sufficiently high surplus electricity production and the lowest LCOE are achieved with the 'bigger-is-better' approach. In locations where seawater temperature variations are high, however, the surplus costs are too high and the lowest LCOE were achieved with slightly less conservative designs.

This study shows that a good understanding of local thermal resources is essential for OTEC's economic performance and design temperatures should not be chosen arbitrarily. OTEC developers should not be tempted to use overly optimistic design temperatures, as the consequently downsized systems performed the worst technically and economically throughout all investigated cases. We validated our model with recent OTEC literature and tested it for various cost assumptions, system sizes, seawater pipe diameters, and seawater temperature profiles across four different locations in Indonesia. Therefore, we believe our insights scale to a global level and future research should consolidate them with more case studies spread across the world.

For a 136 $MW_{gross}$ plant in Ende, the lowest LCOE is 15.12 US¢(2021)/kWh with a final net present value of 49 US$ million against a local tariff of 15.77 US¢(2021)/kWh. We also indicated that large-scale OTEC might be economically attractive for at least eleven other countries. This shows that OTEC's economic feasibility is not bound to niche use cases with exuberantly high electricity prices, but also expands to a broader range of less extreme applications. This could lift the technology to a broader global audience and show policymakers worldwide that OTEC can make a meaningful contribution to the energy transition. This is important as OTEC's development to commercialisation will require global collaboration not only to improve the technology, but also to lay the regulatory groundwork to get OTEC in the water as cost-efficiently as possible. All these efforts should contribute to driving down costs and narrowing the current cost range. If the prohibitively high cost assumptions in literature materialise, it will be difficult to establish economically feasible use cases. To avoid these costs, we recommend further research on seawater pipe materials and manufacturing as well as a thoughtful upscaling of OTEC from land-based to floating systems. Regarding the seawater pipe, we found that using several smaller pipes instead of few large pipes can narrow the gap to the current state of the art and thus increase the technical feasibility of large-scale OTEC. These findings could be further refined by addressing the limitations of our model in future research, namely by (1) capturing the off-design behaviour of the heat exchangers in more detail, (2) adding an objective function to obtain optimised off-design LCOE, (3) exploring further system control schemes, (4) using a more complete set of ocean data, (4) considering wake effects at the tip of the seawater pipes and by (5) using measured field data instead of modelled data.

Generally, the impression arose during this study that OTEC's biggest barrier is not necessarily the technical state of the art, but political commitment. The hard truth is that global OTEC resources are mostly in regions where investment and lobbying power are limited. One can only wonder where OTEC would stand today if there were tangible resources in Europe or the United States. Then again, the world has proven in the past that national interests can be put aside for the greater global good. But whether OTEC can build a strong enough case to spark such an engagement, only time can tell.

### *CRediT authorship contribution statement*

**Jannis Langer:** Conceptualization, Data curation, Formal analysis, Investigation, Writing – original draft. **Carlos Infante Ferreira:** Methodology, Supervision, Validation, Writing – review & editing. **Jaco Quist:** Methodology, Supervision, Writing – review & editing.

### Declaration of Competing Interest

The authors declare that they have no known competing financial interests or personal relationships that could have appeared to influence the work reported in this paper.

### *Acknowledgement*

Work reported in this paper is funded by a grant from the Dutch research council NWO for the project entitled "Regional Development Planning and Ideal Lifestyle of Future Indonesia", under the NWO Merian Fund call on collaboration with Indonesia. Many thanks to Aida Astuti Cahyaningwidi, Nadia Febina from Lumare Energi, and Prof.

Kornelis Blok for interesting discussions and useful feedback.

*Data Availability*

The dataset related to this article can be found under the DOI 10.4121/16438386, hosted at the repository 4TU. Research Data [42].

**Appendix A. Equations used in the design model (I/II). For work and heat, the following sign convention applies: flows into the system are positive, flows out of the system are negative. An alternative, unformatted version of this table can be found in the dataset of this paper.**

| Value | Formula |
|---|---|
| **Saturation Temperature & Pressure, Enthalpy and Entropy of Ammonia ($NH_3$)** | |
| Saturation Temperature $T_{sat}$ [°C] | Evaporation: $T_{evap} = T_{WW,in} - \Delta T_{WW} - \Delta T_{pp}$<br>Condensation: $T_{cond} = T_{CW,in} + \Delta T_{CW} + \Delta T_{pp}$ |
| Saturation pressure $p_{sat}$ [bar] (approximation function based on saturation table) | $p_{sat}(T_{sat}) = 2.196*10^{-5}*T_{sat}^3 + 1.93103*10^{-3}*T_{sat}^2 + 0.1695763*T_{sat} + 4.257339601$ |
| Enthalpy liquid phase $h'$ [kJ/kg] (approximation function based on saturation table) | $h'(p_{sat}) = -0.0235*p_{sat}^4 + 0.9083*p_{sat}^3 - 12.93*p_{sat}^2 + 97.316*p_{sat} - 39.559$ |
| Enthalpy vapour phase $h''$ [kJ/kg] (approximation function based on saturation table) | $h''(p_{sat}) = 28.276*\ln(p_{sat}) + 1418.1$ |
| Entropy liquid phase $s'$ [kJ/kgK] (approximation function based on saturation table) | $s'(p_{sat}) = 0.3947*\ln(p_{sat}) + 0.4644$ |
| Entropy vapour phase $s''$ [kJ/kgK] (approximation function based on saturation table) | $s''(p_{sat}) = -0.352*\ln(p_{sat}) + 6.1284$ |
| **Turbine + Generator + Power Transmission** | |
| Isentropic quality at turbine outlet $x_{turb,out,is}$ [%] | $x_{turb,out,is} = \frac{s_{turb,in} - s'_{turb,out}}{s''_{turb,out} - s'_{turb,out}}$ |
| Isentropic enthalpy at turbine outlet $h_{turb,out,is}$ [kJ/kg] | $h_{turb,out,is} = h'*(1 - x_{turb,out,is}) + h''*x_{turb,out,is}$ |
| Enthalpy at turbine outlet $h_{turb,out}$ [kJ/kg] | $h_{turb,out} = (h_{turb,out,is} - h_{turb,in})*\eta_{is,turb} + h_{turb,in}$ |
| Mass flow ammonia $\dot{m}_{NH_3}$ [kg/s] | $\dot{m}_{NH_3} = \frac{\dot{W}_{t,turb,gross}}{h_{turb,out} - h_{turb,in}}$ |
| Transmission efficiency $\eta_{trans}$ [%] | $\eta_{trans} = 100 - 2*10^{-4}*D^2 - 1.99*10^{-2}*D$ |
| **Ammonia Pump** | |
| Enthalpy at pump outlet $h_{pump,out}$ [kJ/kg] | $h_{pump,out} = \frac{p_{evap} - p_{cond}}{\rho_{NH_3,liq}*\eta_{is,pump}} + h_{pump,in}$ |
| Pump power consumption $\dot{W}_{t,pump,NH_3}$ [kW] | $\dot{W}_{t,pump,NH_3} = \dot{m}_{NH_3}*(h_{pump,out} - h_{pump,in})$ |
| **Evaporator** | |
| Logarithmic temperature difference $\Delta T_{log,evap}$ [K] | $\Delta T_{log,evap} = \frac{((T_{WW,in} - T_{evap}) - ((T_{WW,in} - \Delta T_{WW}) - T_{evap}))}{\ln\left(\frac{(T_{WW,in} - T_{evap})}{((T_{WW,in} - \Delta T_{WW}) - T_{evap})}\right)}$ |
| Evaporation heat $\dot{Q}_{evap}$ [kW] | $\dot{Q}_{evap} = \dot{m}_{NH_3}*(h_{evap,out} - h_{evap,in})$ |
| Mass flow warm seawater $\dot{m}_{WW}$ [kg/s] | $\dot{m}_{WW} = \frac{\dot{Q}_{evap}}{c_{p,H_2O}*\Delta T_{WW}}$ |
| Heat transfer area evaporator $A_{evap}$ [$m^2$] | $A_{evap} = \frac{\dot{Q}_{evap}}{U_{evap}*\Delta T_{log,evap}}$ |
| **Condenser** | |
| Logarithmic temperature difference $\Delta T_{log,cond}$ [K] | $\Delta T_{log,cond} = \frac{((T_{cond} - T_{CW,in}) - (T_{cond} - (T_{CW,in} + \Delta T_{CW})))}{\ln\left(\frac{(T_{cond} - T_{CW,in})}{(T_{cond} - (T_{CW,in} + \Delta T_{CW}))}\right)}$ |
| Condensation heat $\dot{Q}_{cond}$ [kW] | $\dot{Q}_{cond} = \dot{m}_{NH_3}*(h_{cond,out} - h_{cond,in})$ |
| Mass flow cold seawater $\dot{m}_{CW}$ [kg/s] | $\dot{m}_{CW} = \frac{\lvert\dot{Q}_{cond}\rvert}{c_{p,H_2O}*\Delta T_{CW}}$ |
| Heat transfer area condenser $A_{cond}$ [$m^2$] | $A_{cond} = \frac{\lvert\dot{Q}_{cond}\rvert}{U_{cond}*\Delta T_{log,cond}}$ |

**Appendix B. Equations used in the design model (II/II). For work and heat, the following sign convention applies: Flows into the system are positive, flows out of the system are negative. An alternative, unformatted version of this table can be found in the dataset of this paper.**

| **Seawater Pipes (for both WW and CW)** | |
|---|---|
| Required total inner pipe area $A_{tot}$ [$m^2$] | $A_{tot} = \frac{\dot{m}_{WW/CW}}{\rho_{H2O}*v_{WW/CW}}$ |
| Inner diameter $d_{pipe}$ [m] | |
| Number of pipes $N_{pipe}$ [-] | |

(*continued on next page*)

(*continued*)

| | |
|---|---|
| **Seawater Pipes (for both WW and CW)** | |
| | $d_{pipe} = \sqrt{\frac{4*A_{tot}}{\pi*N_{pipe}}}$ |
| | Increase $N_{pipe}$ in steps of 1 until $d_{pipe} \leq d_{max}$ |
| Mass of pipes $m_{pipe}$ [kg] | $m_{pipe} = \frac{\pi}{4}*\left(\left(d_{pipe}+2*t\right)^2 - d_{pipe}^2\right)*l_{pipe}*\rho_{HDPE/FPR}*N_{pipe}$ |
| Dynamic viscosity seawater $\mu$ [Pa*s]<br>(Approximation function based on state table) | $\mu = 3.443*10^{-7}*T^2 - 4.711*10^{-5}*T + 1.767*10^{-3}$ |
| Reynolds number $Re$ [-] | $Re = \frac{\rho_{WW/CW}*v_{WW/CW}*d_{pipe}}{\mu_{WW/CW}}$ |
| Darcy friction factor $f_D$ [-]<br>(Swamee-Jain equation) | $f_D = \frac{0.25}{\left(\log_{10}\left(\frac{z}{3.7*d_{pipe}} + \frac{5.74}{Re^{0.9}}\right)\right)^2}$ |
| Pressure drop in pipe $\Delta p_{pipe}$ [Pa] | $\Delta p_{pipe} = f_D*\rho_{WW/CW}*\frac{l_{pipe}}{d_{pipe}}*\frac{v_{pipe}^2}{2}$ |
| Pressure drop in heat exchanger $\Delta p_{evap/cond}$ [Pa] | $\Delta p_{evap/cond} = \rho_{WW/CW}*\frac{v_{evap/cond}^2}{2}*K_{L,evap/cond}$ |
| Power consumption seawater pump $\dot{W}_{t,pump}$ [kW] | $\dot{W}_{t,pump} = \frac{\dot{m}_{CW}*\left(\Delta p_{pipe} + \Delta p_{evap,cond}\right)}{\rho_{H2O}*\eta_{is,pump}}$ |
| **Net Power and Efficiency** | |
| Net Power Production $\dot{W}_{t,net}$ [kW] | $\dot{W}_{t,net} = \dot{W}_{t,turb,gross}*\eta_{mech,turb}*\eta_{el,turb}*\eta_{trans} + \frac{\dot{W}_{t,pump,NH_3} + \dot{W}_{t,pump}}{\eta_{el,pump}}$ |
| Net Thermal Efficiency $\eta_{net}$ [%] | $\eta_{net} = \frac{\left\lvert\dot{W}_{t,net}\right\rvert}{\dot{Q}_{evap}}$ |
| **Exergy Analysis, Carnot Efficiency, and Second Law Efficiency** | |
| Dead-State Temperature $T_0$ [K] | $T_0 = \frac{T_{CW,out} - T_{CW,in}}{\ln\left(\frac{T_{CW,out}}{T_{CW,in}}\right)}$ |
| Net Exergy Change $\Delta Ex$ [kW] | $\Delta Ex = \dot{m}*[(h_{out} - h_{in}) - T_0*(s_{out} - s_{in})]$ |
| Net Exergy Efficiency $\eta_{ex,net}$ [%]<br>($Ex_{in}$ is the exergy inflow from the surface water in the evaporator) | $\eta_{ex,net} = \frac{\left\lvert\dot{W}_{t,net}\right\rvert}{Ex_{in}}$ |
| Logarithmic Mean Surface Seawater Temperature $T_{log,WW}$ [K] | $T_{log,WW} = \frac{T_{WW,out} - T_{WW,in}}{\ln\left(\frac{T_{WW,out}}{T_{WW,in}}\right)}$ |
| Carnot Efficiency $\eta_{Carnot}$ [%] | $\eta_{Carnot} = 1 - \frac{T_0}{T_{log,WW}}$ |
| Second Law Efficiency $\eta_{2ndlaw}$ [%] | $\eta_{2ndlaw} = \frac{\eta_{net}}{\eta_{Carnot}}$ |
| **LCOE** | |
| Capital Recovery Factor $CRF$ [%] | $CRF = \frac{DR*(1+DR)^n}{(1+DR)^n - 1}$ |
| Scaled specific capital expenses $capex$ [US$ million/unit] | $capex_i = capex_0*\left(\frac{\dot{W}_{t,gross,0}}{\dot{W}_{t,gross,i}}\right)^b$ |
| CAPEX without extra costs [US$ million] (sum of $H$ cost components. Unit can be gross power output, power consumption, mass or area) | $CAPEX_{noextra} = \sum_{h=1}^{H} capex_h*unit_h$ |
| Total $CAPEX$ [US$ million] | $CAPEX_{total} = CAPEX_{noextra}*(1 + perc_{ext})$ |
| Annual Electricity Production $AEP$ [kWh/year]<br>(Sum of all 3-hour power outputs in a year. For leap years: $M = 2{,}928$; for non-leap years: $M = 2{,}920$) | On-Design Model:<br>$AEP = \left\lvert\dot{W}_{t,net}\right\rvert*c_f*8760$<br>Off-Design Model:<br>$AEP = \sum_m^M \dot{W}_{t,net,m}*3$ |
| Levelized Cost of Electricity $LCOE$ [US¢/kWh]<br>Annual Electricity Production $AEP$ in year $i$ calculated by off-design model in steps 6 and 7 in Fig. 1. | On-Design LCOE:<br>$LCOE = \frac{CRF*CAPEX + OPEX}{AEP}$<br>Off-Design LCOE:<br>$LCOE = \frac{\sum_{i=1}^{n} \frac{CAPEX_{total,i} + OPEX_i}{(1+DR)^i}}{\sum_{i=1}^{n} \frac{AEP_i}{(1+DR)^i}}$ |

**Appendix C. Comparison of correlations between heat exchanger channel velocity and overall heat transfer coefficient used in Bernardoni et al. [3]. Original refers to the correlations presented in the original study. The correlations were adjusted with a correction factor to yield the same overall heat transfer coefficients at 1.0 m/s channel velocity.**

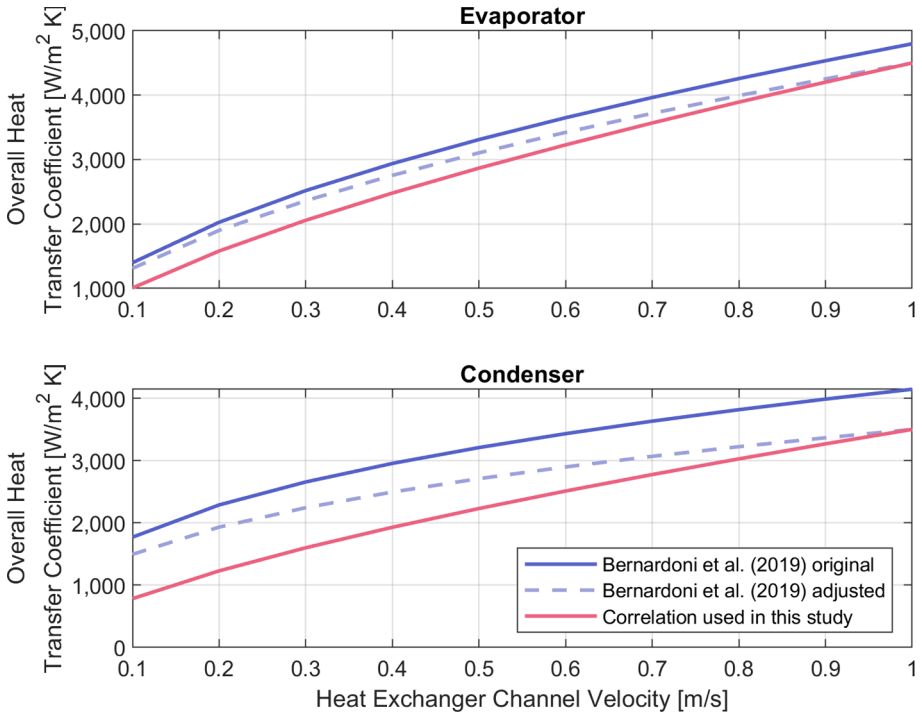


**Appendix D. (a) cleaned 19-year surface and deep-sea water temperature profiles in Jayapura, Indonesia. Outliers are removed from the profiles using box and whisker plots for (b) surface seawater temperature and (c) deep-sea water.**

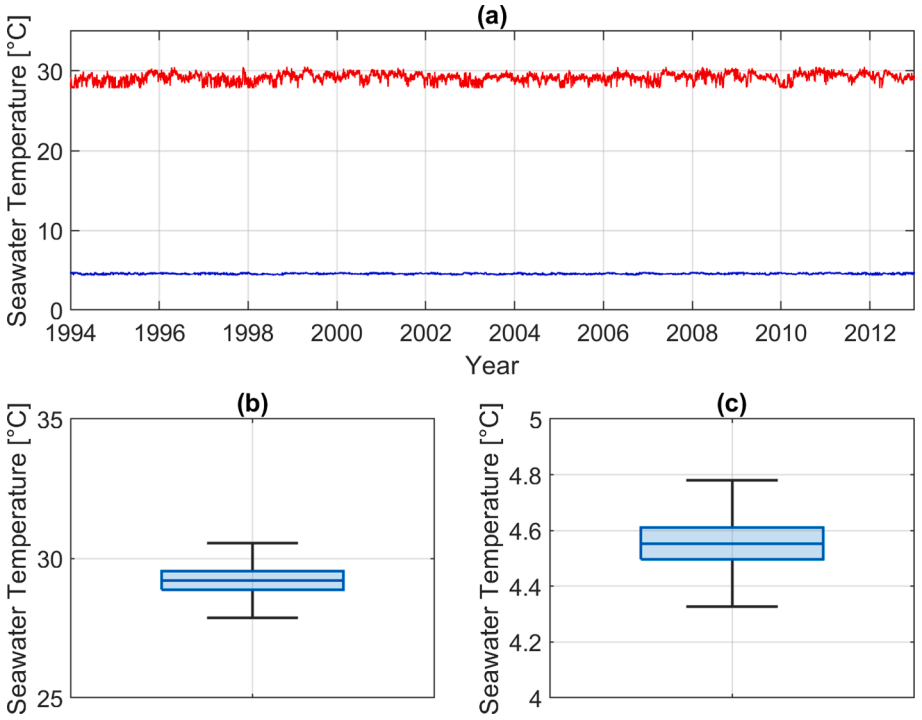

**Appendix E. (a) cleaned 19-year surface and deep-sea water temperature profiles in Tarakan, Indonesia. Outliers are removed from the profiles using box and whisker plots for (b) surface seawater temperature and (c) deep-sea water.**

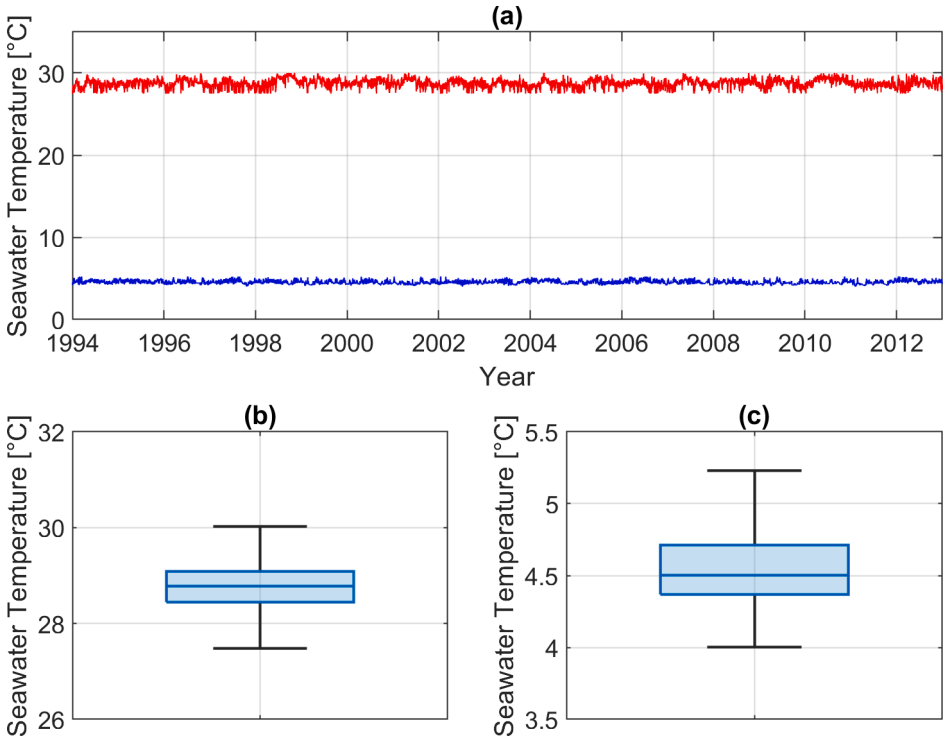


**Appendix F. (a) cleaned 19-year surface and deep-sea water temperature profiles in Sabang, Indonesia. Outliers are removed from the profiles using box and whisker plots for (b) surface seawater temperature and (c) deep-sea water.**

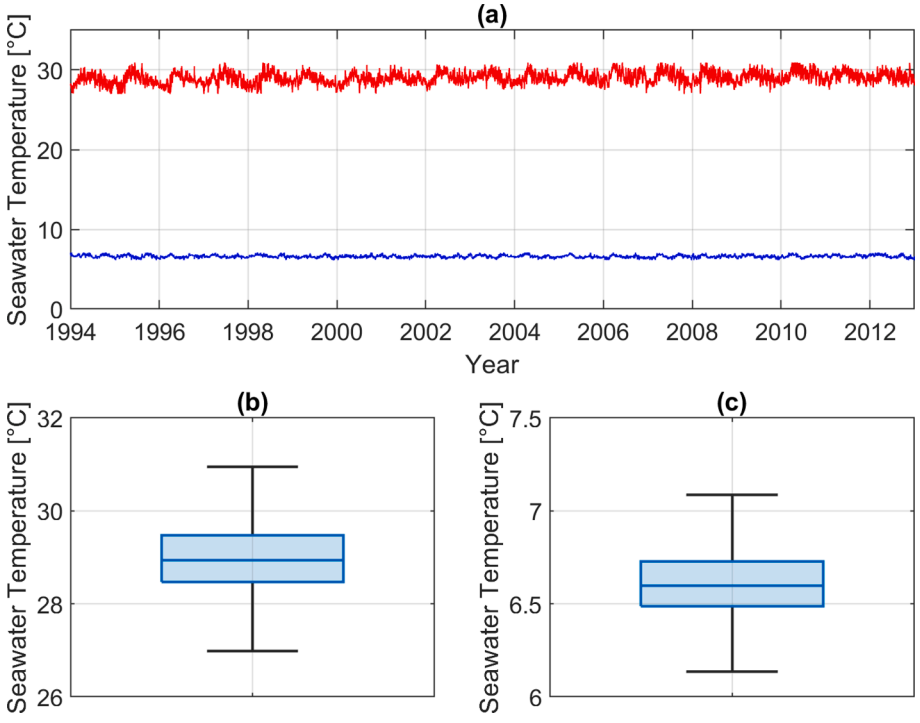

**Appendix G. System designs for 136 $MW_{gross}$ for all nine temperature configurations and high-cost assumptions in Ende. Only configuration 5 differs from the configurations with low-cost assumptions shown in Table 4 in the main text.**

| | Configuration with High-Cost Assumptions | | | | | | | | |
|---|---|---|---|---|---|---|---|---|---|
| | 1 (Min WW+Max CW) | 2 (Med WW+Max CW) | 3 (Max WW+Max CW) | 4 (Min WW+Med CW) | 5 (Med WW+Med CW) | 6 (Max WW+Med CW) | 7 (Min WW+Min CW) | 8 (Med WW+Min CW) | 9 (Max WW+Min CW) |
| | **Energy Balance (units in MW if not stated otherwise)** | | | | | | | | |
| Heat Evaporator | 5,551 | 4,150 | 3,506 | 4,979 | 3,983 | 3,387 | 5,020 | 4,008 | 3,298 |
| Heat Condenser | −5,417 | −4,016 | −3,372 | −4,845 | −3,849 | −3,253 | −4,886 | −3,874 | −3,164 |
| Gross Power Turbine | −136 | −136 | −136 | −136 | −136 | −136 | −136 | −136 | −136 |
| Power $NH_3$ Pump | 1.9 | 2.0 | 2.1 | 1.9 | 2.0 | 2.1 | 1.8 | 2.0 | 2.1 |
| Power WW Pump | 26.3 | 15.3 | 11.6 | 23.6 | 14.7 | 11.2 | 20.8 | 13.3 | 10.9 |
| Power CW Pump | 21.7 | 14.5 | 12.3 | 21.8 | 13.9 | 11.9 | 22.0 | 14.0 | 11.6 |
| Losses $NH_3$ Pump | 0.1 | 0.1 | 0.1 | 0.1 | 0.1 | 0.1 | 0.1 | 0.1 | 0.1 |
| Losses Turbine and Transmission | 13.5 | 13.5 | 13.5 | 13.5 | 13.5 | 13.5 | 13.5 | 13.5 | 13.5 |
| Net Power Turbine at Shore | −72.6 | −90.6 | −96.4 | −75.2 | −91.8 | −97.2 | −77.8 | −93.2 | −97.9 |
| Net Thermal Efficiency [%] | 1.3% | 2.2% | 2.8% | 1.5% | 2.3% | 2.9% | 1.5% | 2.3% | 3.0% |
| | **Exergy Balance (units in MW if not stated otherwise)** | | | | | | | | |
| Exergy Inflow Evaporator | 275 | 256 | 244 | 259 | 252 | 241 | 264 | 256 | 239 |
| Exergy Loss Evaporator | −38.1 | −35.1 | –32.5 | –33.7 | –33.6 | −31.3 | −37.8 | −36.8 | −30.4 |
| Exergy Loss Turbine | −29.5 | −29.4 | −29.4 | −29.5 | −29.4 | −29.4 | −29.5 | −29.4 | −29.4 |
| Exergy Loss Condenser | −73.0 | −57.4 | −48.2 | −61.7 | −55.3 | −46.7 | −62.5 | −55.9 | −45.6 |
| Exergy Loss $NH_3$ Pump | −0.1 | −0.1 | −0.1 | −0.1 | −0.1 | −0.1 | −0.1 | −0.1 | −0.1 |
| Exergy Loss WW Pump | −26.3 | −15.3 | −11.6 | –23.6 | −14.7 | −11.2 | −20.8 | −13.3 | −10.9 |
| Exergy Loss CW Pump | −21.7 | −14.5 | −12.3 | −21.8 | −13.9 | −11.9 | –22.0 | −14.0 | −11.6 |
| Exergy Loss Conversion Losses | −13.5 | −13.5 | −13.5 | −13.5 | −13.5 | −13.5 | −13.5 | −13.5 | −13.5 |
| Exergy Outflow at Shore | −72.6 | −90.6 | −96.4 | −75.2 | −91.8 | −97.2 | −77.8 | −93.2 | −97.9 |
| Net Exergy Efficiency [%] | 26.4% | 35.4% | 39.5% | 29.0% | 35.6% | 40.3% | 29.5% | 36.4% | 40.9% |
| Carnot Efficiency [%] | 4.9% | 6.2% | 7.0% | 5.2% | 6.2% | 7.1% | 5.3% | 6.4% | 7.3% |
| Second Law Efficiency [%] | 26.4% | 35.4% | 39.5% | 29.0% | 35.6% | 40.3% | 29.5% | 36.4% | 40.9% |
| | **Mass Flows** | | | | | | | | |
| Mass Flow $NH_3$ [kg/s] | 4,523 | 3,379 | 2,850 | 4,043 | 3,237 | 2,749 | 4,073 | 3,254 | 2,673 |
| Mass Flow WW [kg/s] | 396,531 | 230,564 | 175,284 | 355,627 | 221,260 | 169,357 | 313,781 | 200,403 | 164,899 |
| Mass Flow CW [kg/s] | 300,962 | 200,808 | 168,589 | 302,789 | 192,434 | 162,661 | 305,395 | 193,702 | 158,202 |
| | **Temperature Changes** | | | | | | | | |
| Temperature Change WW [K] | 3.5 | 4.5 | 5.0 | 3.5 | 4.5 | 5.0 | 4.0 | 5.0 | 5.0 |
| Temperature Change CW [K] | 4.5 | 5.0 | 5.0 | 4.0 | 5.0 | 5.0 | 4.0 | 5.0 | 5.0 |
| | **Evaporator and Condenser** | | | | | | | | |
| Area Evaporator [$m^2$] | 530,146 | 349,381 | 279,171 | 475,458 | 335,283 | 269,730 | 448,899 | 319,177 | 262,630 |
| Evaporation Temperature [°C] | 19.2 | 22.8 | 25.1 | 19.2 | 22.8 | 25.1 | 18.7 | 22.3 | 25.1 |
| Evaporation Pressure [bar] | 8.4 | 9.4 | 10.1 | 8.4 | 9.4 | 10.1 | 8.2 | 9.2 | 10.1 |
| Area Condenser [$m^2$] | 586,360 | 411,201 | 345,223 | 556,938 | 394,052 | 333,084 | 561,731 | 396,648 | 323,954 |
| Condensation Temperature [°C] | 10.6 | 11.1 | 11.1 | 9.6 | 10.6 | 10.6 | 9.2 | 10.2 | 10.2 |
| | 6.3 | 6.4 | 6.4 | 6.1 | 6.3 | 6.3 | 6.0 | 6.2 | 6.2 |

(*continued on next page*)

(*continued*)

| | Configuration with High-Cost Assumptions | | | | | | | | |
|---|---|---|---|---|---|---|---|---|---|
| | **1 (Min WW+Max CW)** | **2 (Med WW+Max CW)** | **3 (Max WW+Max CW)** | **4 (Min WW+Med CW)** | **5 (Med WW+Med CW)** | **6 (Max WW+Med CW)** | **7 (Min WW+Min CW)** | **8 (Med WW+Min CW)** | **9 (Max WW+Min CW)** |
| Condensation Pressure [bar] | | | | | | | | | |
| | **Seawater Pipes** | | | | | | | | |
| Diameter CW Pipes [m] | 7.9 | 7.9 | 7.2 | 7.9 | 7.7 | 7.1 | 7.9 | 7.7 | 7.0 |
| Number of CW Pipes | 6 | 4 | 4 | 6 | 4 | 4 | 6 | 4 | 4 |
| Diameter WW Pipes [m] | 7.9 | 6.9 | 7.4 | 7.4 | 6.8 | 7.3 | 7.0 | 7.9 | 7.2 |
| Number of WW Pipes | 8 | 6 | 4 | 8 | 6 | 4 | 8 | 4 | 4 |

## References


[1] Langer J, Quist J, Blok K. Recent progress in the economics of ocean thermal energy conversion: Critical review and research agenda. Renew Sustain Energy Rev 2020;130:109960. https://doi.org/10.1016/j.rser.2020.109960.

[2] Langer J, Quist J, Blok K. Upscaling scenarios for ocean thermal energy conversion with technological learning in Indonesia and their global relevance. Under Rev 2021.

[3] Bernardoni C, Binotti M, Giostri A. Techno-economic analysis of closed OTEC cycles for power generation. Renew Energy 2019;132:1018–33. https://doi.org/10.1016/j.renene.2018.08.007.

[4] Fuller RD. Ocean thermal energy conversion: technology brief. Abu Dhabi 1978;4 (2-4):241–58. https://doi.org/10.1016/0302-184X(78)90026-4.

[5] Petterson MG, Kim HJ. Can Ocean Thermal energy conversion and seawater utilisation assist small island developing states? A Case study of Kiribati, Pacific Islands Region. In: Kim AS, Kim H-J, editors. Ocean Therm. Energy Convers. - Past, Present. Prog., IntechOpen; 2020. Doi: 10.5772/intechopen.91945.

[6] International Renewable Energy Agency. Innovation outlook: Ocean energy technologies; 2020.

[7] Vega LA. Ocean thermal energy conversion. Encycl Sustain Sci Technol 2012: 7296–328. https://doi.org/10.1007/978-1-4419-0851-3.

[8] Rajagopalan K, Nihous GC. Estimates of global Ocean Thermal Energy Conversion (OTEC) resources using an ocean general circulation model. Renew Energy 2013; 50:532–40. https://doi.org/10.1016/j.renene.2012.07.014.

[9] Martel L, Smith P, Rizea S, Van Ryzin J, Morgan C, Noland G, et al. Ocean thermal energy conversion life cycle cost assessment. Final Technical Report 2012;161.

[10] Giostri A, Romei A, Binotti M. Off-design performance of closed OTEC cycles for power generation. Renew Energy 2021;170:1353–66. https://doi.org/10.1016/j.renene.2021.02.047.

[11] Hernández-Romero IM, Nápoles-Rivera F, Flores-Tlacuahuac A, Fuentes-Cortés LF. Optimal design of the ocean thermal energy conversion systems involving weather and energy demand variations. Chem Eng Process – Process Intensif 2020;157: 108114. https://doi.org/10.1016/j.cep.2020.108114.

[12] Soto R, Vergara J. Thermal power plant efficiency enhancement with Ocean Thermal Energy Conversion. Appl Therm Eng 2014;62(1):105–12. https://doi.org/10.1016/j.applthermaleng.2013.09.025.

[13] Garduño-Ruiz EP, Silva R, Rodríguez-Cueto Y, García-Huante A, Olmedo-González J, Martínez ML, et al. Criteria for Optimal Site Selection for Ocean Thermal Energy Conversion (OTEC) Plants in Mexico. Energies 2021;14(8):2121. https://doi.org/10.3390/en14082121.

[14] Global CCS Institute. Energy Use in the Pacific Region; 2013.

[15] Seungtaek L, Hosaeng L, Junghyun M, Hyeonju K. Simulation data of regional economic analysis of OTEC for applicable area. Processes 2020;8(9):1107. https://doi.org/10.3390/pr8091107.

[16] Vega LA. Economics of Ocean Thermal Energy Conversion (OTEC): An Update. Offshore Technol Conf 2010:3–6. https://doi.org/10.4043/21016-MS.

[17] Langer J, Cahyaningwidi AA, Chalkiadakis C, Quist J, Hoes O, Blok K. Plant siting and economic potential of ocean thermal energy conversion in Indonesia a novel GIS-based methodology. Energy 2021;224:120121. https://doi.org/10.1016/j.energy.2021.120121.

[18] Asian Development Bank. Achieving Universal Electricity Access in Indonesia. Mandaluyong City; 2016.

[19] Ministry of Energy and Mineral Resources. Besaran Biaya Pokok Penyediaan Pembangkitan PT Perusahaan Listrik Negara (Persero); 2019.

[20] Ahmadi P, Dincer I, Rosen MA. Performance assessment of a novel solar and ocean thermal energy conversion based multigeneration system for coastal areas. J Sol Energy Eng Trans ASME 2015;137. https://doi.org/10.1115/1.4028241.

[21] Zhou S, Liu X, Bian Y, Shen S. Energy, exergy and exergoeconomic analysis of a combined cooling, desalination and power system. Energy Convers Manag 2020; 218:113006. https://doi.org/10.1016/j.enconman.2020.113006.

[22] Sharqawy MH, Lienhard VJH, Zubair SM. Thermophysical properties of seawater: A review of existing correlations and data. Desalin Water Treat 2011;29:355. https://doi.org/10.5004/dwt.2011.2947.

[23] Upshaw CR. Thermodynamic and Economic Feasibility Analysis of a 20 MW Ocean Thermal Energy Conversion (OTEC) Power. University of Texas at Austin; 2012.

[24] Sinnott R, Towler G. Chemical engineering design. 6th ed. Elsevier; 2020.

[25] Bharathan D. Staging Rankine Cycles Using Ammonia for OTEC Power Production. 2011. Doi: 10.2172/1010862.

[26] Vera D, Baccioli A, Jurado F, Desideri U. Modeling and optimization of an ocean thermal energy conversion system for remote islands electrification. Renew Energy 2020;162:1399–414. https://doi.org/10.1016/j.renene.2020.07.074.

[27] Vega LA, Michaelis D. First generation 50 MW OTEC plantship for the production of electricity and desalinated water. Proc Annu Offshore Technol Conf 2010;4: 2979–95. https://doi.org/10.4043/20957-ms.

[28] Lockheed Martin. NAVFAC Ocean Thermal Energy Conversion (OTEC) Project 2011;4:274.

[29] Bosch J, Staffell I, Hawkes AD. Global levelised cost of electricity from offshore wind. Energy 2019;189:116357. https://doi.org/10.1016/j.energy.2019.116357.

[30] Jung J-Y, Lee HS, Kim H-J, Yoo Y, Choi W-Y, Kwak H-Y. Thermoeconomic analysis of an ocean thermal energy conversion plant. Renew Energy 2016;86:1086–94. https://doi.org/10.1016/j.renene.2015.09.031.

[31] Keesmaat K. Installation of a Large Diameter Cold Water Pipe in Deepwater for a Land-Based OTEC Plant. Delft University of Technology; 2015.

[32] Adiputra R, Utsunomiya T, Koto J, Yasunaga T, Ikegami Y. Preliminary design of a 100 MW-net ocean thermal energy conversion (OTEC) power plant study case: Mentawai island, Indonesia. J Mar Sci Technol 2020;25(1):48–68. https://doi.org/10.1007/s00773-019-00630-7.

[33] Oko COC, Obeneme WB. Thermo-economic analysis of an ocean thermal power plant for a Nigerian coastal region. Int J Ambient Energy 2018;39(6):562–72. https://doi.org/10.1080/01430750.2017.1318789.

[34] Bureau of Labour Statistics. CPI Inflation Calculator 2021. https://data.bls.gov/cgi-bin/cpicalc.pl?cost1=1.00&year1=201801&year2=202101 (accessed May 19, 2021).

[35] Tao X, Dahlgren E, Leichsenring M, Infante Ferreira CA. $NH_3$ condensation in a plate heat exchanger: experimental investigation on flow patterns, heat transfer and frictional pressure drop. Int J Heat Mass Transf 2020;151:119374. https://doi.org/10.1016/j.ijheatmasstransfer.2020.119374.

[36] Tao X. $NH_3$ Condensation within Plate Heat Exchangers: Flow patterns, Heat Transfer & Frictional pressure drop. Delft University of Technology; 2021. Doi: 10.4233/uuid.

[37] GEBCO Compilation Group. GEBCO 2020 Grid 2020. Doi: doi:10.5285/a29c5465-b138-234d-e053-6c86abc040b9.

[38] Vega LA, Nihous GC. Design of a 5 MWe OTEC Pre-Commercial Plant. Proc. Oceanol. Int. '94 Conf., Brighton; 1994.

[39] Rahmawati S, Muna AI, Wardhana W. Economic study on the construction of a 50 MW Ocean Thermal Energy Conversion (OTEC) facility in Banten Province, Indonesia. IOP Conf Ser: Earth Environ Sci 2021;649(1):012015. https://doi.org/10.1088/1755-1315/649/1/012015.

[40] Lavidas G, Venugopal V. Prospects and applicability of wave energy for South Africa. Int J Sustain Energy 2018;37(3):230–48. https://doi.org/10.1080/14786451.2016.1254216.

[41] Lavidas G, Blok K. Shifting wave energy perceptions: The case for wave energy converter (WEC) feasibility at milder resources. Renew Energy 2021;170:1143–55. https://doi.org/10.1016/j.renene.2021.02.041.

[42] Langer J, Infante Ferreira CA, Quist J. Data Underlying the Paper "Is bigger always better? Designing economically feasible ocean thermal energy conversion systems using spatio-temporal resource data" 2021. doi:10.4121/16438386.